SPECIAL SOLUTIONS OF THE BOHR HAMILTONIAN WITH THE WOODS-SAXON POTENTIAL

Ph.D. Thesis

in

Engineering Physics

University of Gaziantep

Supervisor:

Prof. Dr. Bülent GÖNÜL

by

Mustafa ÇAPAK

July 2015

©2015[Çapak, M.]

T.C.
UNIVERSITY OF GAZİANTEP
GRADUATE SCHOOL OF
NATURAL & APPLIED SCIENCES
ENGINEERING PHYSICS

Name of the Thesis : SPECIAL SOLUTIONS OF THE BOHR HAMILTONIAN WITH THE WOODS-SAXON POTENTIAL
Name of the student : Mustafa ÇAPAK
Exam Date : 30/07/2015

Approval of the Graduate School of Natural and Applied Sciences

Prof. Dr. Metin BEDİR
Director

I certify that this thesis satisfies all the requirements as a thesis for the degree of Doctor of Philosophy.

Prof. Dr. A. Necmeddin YAZICI
Head of Department

This is to certify that we have read this thesis and that in our opinion it is fully adequate, in scope and quality, as a thesis for the degree of Doctor of Philosophy.

Prof. Dr. Bülent GÖNÜL
Supervisor

Examining Committee Members	signature
Prof. Dr. Fahir T. AKYILDIZ	
Prof. Dr. Bülent GÖNÜL	
Assoc. Prof. Dr. Cumhur CANBAZOĞLU	
Assist. Prof. Dr. Hümbet AHMEDOV	
Assist. Prof. Dr. İlyas İNCİ	

I hereby declare that all information in this document has been obtained and presented in accordance with academic rules and ethical conduct. I also declare that, as required by these rules and conduct, I have fully cited and referenced all material and results that are not original to this work.

Mustafa ÇAPAK

ABSTRACT

SPECIAL SOLUTIONS OF THE BOHR HAMILTONIAN WITH THE WOODS-SAXON POTENTIAL

ÇAPAK, Mustafa
Ph.D. in Engineering of Physics
Supervisor: Prof. Dr. Bülent GÖNÜL
30 July 2015, 61 pages

The recent influential studies on the nuclear structure have focused on the quantum shape phase transitions of atomic nuclei within the frame of the Collective Model, which have enabled many researchers to test the reliability of the models used.

As the special solutions of the Bohr Hamiltonian dealing with collective behaviour of the nucleus in terms of collective variables β and γ in five-dimension, E(5) and X(5) are the most important critical point symmetries, which describe the shape phase transition between vibrational and $\gamma-$unstable/axially symmetric prolate rotor, respectively. Hence, for the first time in the related literature, considering both E(5) and X(5) critical point symmetries, the Bohr Hamiltonian with the well-known Woods-Saxon potential involving the repulsive angular momentum barrier in the non-relativistic domain is solved analytically. We observe that the corresponding new solution well reproduces energy spacing within the ground state and γ bands for more than 100 even-even deformed nuclei, and gives an insight to the physically acceptable parameters that is required for reliable and accurate calculations.

Keywords: Quantum Phase Transitions; Woods-Saxon Potential; Collective Model; Bohr Hamiltonian

ÖZ

WOODS-SAXON POTANSİYELİ İÇEREN BOHR HAMİLTONİYENİNİN ÖZEL ÇÖZÜMLERİ

ÇAPAK, Mustafa
Doktora Tezi, Fizik Mühendisliği Bölümü
Danışman: Prof. Dr. Bülent GÖNÜL
30 Temmuz 2015, 61 sayfa

Kollektif Model çerçevesinde atom çekirdeğinin yapısını açıklamaya yönelik son etkin çalışmalar, kullanılan modellerin güvenilirliğini test edebilmek için birçok araştırmacıya imkan veren, çekirdeğin kuantum şekil faz geçişlerine odaklanmaktadır.

Beş boyutta β ve γ kollektif değişkenleri cinsinden çekirdeğin kollektif davranışı ile ilgilenen Bohr Hamiltoniyeninin özel çözümleri olarak E(5) ve X(5), sırasıyla çekirdeğin titreşim durumundan γ-kararsız/eksenel simetrik prolate rotor durumu arasındaki şekil faz geçişlerini tanımlayan en önemli kritik nokta simetrileridir. Bundan dolayı, ilgili literatürde ilk uygulama olmak üzere, E(5) ve X(5) kritik nokta simetrilerinin her ikisi de ele alınarak, açısal momentum bariyeri içeren bilindik Woods-Saxon potansiyeline sahip Bohr Hamiltoniyeni relativistik olmayan durumlar için analitik olarak çözüldü. İlgili yeni çözümün, 100 den fazla çift-çift çekirdek için temel seviye ve γ bandları içindeki enerji aralıklarını başarılı şekilde ürettiği ve güvenli, kesin hesaplamalar için gereken fiziksel olarak kabul edilebilir parametrelere içerik kazandırdığı gözlemlendi.

Anahtar Kelimeler: Kuantum Faz Geçişleri; Woods-Saxon Potansiyeli; Kollektif Model; Bohr Hamiltoniyeni

I dedicated this work to scientific determination

ACKNOWLEDGEMENTS

Foremost, I would like to express my appreciation to my beloved wife Serpil and daughter Ecrin Nehir for their supports and patience in this exhausting Ph.D. process throughout the sleepless nights. I am grateful also to my dear mother Dudu and father Ahmet, who passed away in 2008, for their unconditional supports.

I will forever be thankful to my advisor Prof. Dr. Bülent GÖNÜL. The moment I met with him is the turning point for my life. He has taught of me not only physics, mathematics, but also fighting against difficulties, finding the truth in a scientific way, optimism and the others whose names I cannot list here. I would have not been able to complete the thesis work without his invaluable guidance.

I wish also to express my sincere appreciation to those who have contributed to build this thesis work during the past five years. Firstly, very special thanks to Prof. Dr. Dennis BONATSOS, whose support from miles and miles away was vital in achieving the present work. In addition, my thanks also go to Prof. Dr. İsmail BOZTOSUN, Assist. Prof. Dr. İlyas İNCİ, Assoc. Prof. Dr. Ahmet BİNGÜL, Assoc. Prof. Dr. Orhan BAYRAK for their recommendations, aids and constructive criticisms.

I am also indebted to the Scientific and Technical Research Council of Turkey(TÜBİTAK) for the financial support under the project number ARDEB/1002-113F218.

Finally, but most importantly, I thank to God for everything I have...

TABLE of CONTENTS

LIST of TABLES

LIST of FIGURES

CHAPTER 1

INTRODUCTION

The quantum phase transitions between different shapes of ground state depending on the change of nucleon number in atomic nuclei constitute an important branch within studies on the nuclear structure analysis. The quantum phase transitions occur as the result of deviation the number of nucleons from closed-shell configuration in which nucleus has equilibrium shape. While atomic nuclei around the closed-shell have almost a spherical shape, in the regions away from the nucleon numbers of the closed-shell, they undergo deformation on their shape [1]. In the deformations, the spectral structure and electric quadrupole transitions (B(E2)) between energy levels are important arguments for examining the Collective Model developed by Bohr and Mottelson in 1950's [2-4].

In the beginning of 2000's the critical point symmetries developed by Iachello [5,6] triggered a lot of studies on the topic in the following years. The critical point symmetries labelled as E(5) and X(5) describe the shape phase transitions between vibrational and γ- unstable/prolate deformed rotational nuclei, respectively. In the both two cases, to reach analytical special solutions, the Bohr Hamiltonian is used as a kind of Schrödinger Equation explaining the collective behaviour of the nucleus with collective variables β and γ, as well as the three Euler angles, in five-dimension. Using an infinite well potential depending on β-variable for both cases, the separation of variables is achieved in the E(5) case by assuming that the potential is independent of γ- variable, while the related X(5) case involves an harmonic oscillator like potential for γ- variable [5,6]. The underlying fact of using infinite well potential for both two cases is that the potential is expected to be flat around the point where shape phase transitions occur.

In addition, to explain the spectral structure of medium mass and heavy even-even nuclei, many physicists have used different potentials, especially in the β-part of the Bohr Hamiltonian [7-12, and the related references therein] in the critical point symmetries. Investigating the corresponding potentials performed so far, one can see that these potentials have common mathematical properties, some of which are to have flat minimum and sloped walls. Along this line, the Woods-Saxon potential is a good candidate [13], which is the main aim of the present work.

Although the Woods-Saxon potential has been used frequently in different fields of nuclear physics, which has not been considered in this context so far due to its non-exactly solvable form in three-dimension. Nevertheless, we show clearly in this thesis work, as a first application in the related literature, this kind of interaction potential leads us to reliable analytical solutions in five-dimension within the frame of Bohr Hamiltonian with a proper use of the usual Pekeris approximation [14] for the related angular momentum barrier. Considering the standard the *s*-wave solution of the Woods-Saxon potential [15] and ongoing debates on it in the literature [16-19], together with the recent comprehensive works [20,21] on such interactions, we first deal with the problem in three-dimension by giving the corresponding solutions in an explicit form.

As the Bohr Hamiltonian has five freedom degree consisting of two collective variables, β and γ, and three Euler angles, θ_i, it offers appropriate solutions to the Woods-Saxon potential with angular momentum like barrier in higher dimensions, which is the starting point for the the present work based on five dimensional solutions. For this reason, we start first with the reliable analytic solutions of the Woods-Saxon potential in 3-dimension within the framework of non-relativistic physics due to the structure of the Bohr Hamiltonian. Considering an interesting connection between the generalized Woods-Saxon potential discussed in Ref.[20] and the standard Woods-Saxon potential involving the repulsive angular momentum barrier in the non-relativistic domain, approximate solutions to the potential are obtained here in this work for any l- levels. With the expertise gained from this discussion, the potential of interest will then be successfully applied to nuclear structure calculations in the frame of the critical point symmetries.

Overall, through the thesis work, we observe that the corresponding new analytical solutions of the Bohr Hamiltonian discussed in detail in our novel work, for both the γ – unstable and prolate deformed cases, produces bandheads and energy spacings well within the bands of more than 100 medium mass and heavy even-even nuclei. Nevertheless, due to some mathematical constraints naturally arisen in the present formalism and the absence of singular behaviour of the Woods-Saxon potential near the origin, the reliable approximate solutions can be obtained only for the lowest bands in the frame of both E(5) and X(5) cases. However, the fitting procedure used through the present work to predict physically meaningful potential parameters leads us to the quite good results which are in a remarkable agreement with the experimental data. Within this context, Chapter 2 discusses the required theoretical background to give the reader the necessary initial physical information as a base in this area. Chapter 3 involves our application results, together with their analysis and discussions, within the framework of the present model. Final Chapter presents some concluding remarks and outlook for the completeness of the work presented in this thesis.

CHAPTER 2

THEORETICAL BACKGROUND

2.1 COLLECTIVE MODEL

Although the liquid drop model and the shell model have tried to explain the nuclear structure in different perspectives individually, neither of them can give a suitable explanation as a whole. While the liquid drop model is successful in predicting the binding energies, it cannot estimate the nuclear magic numbers. On the other hand, the shell model leads us to excellent results regarding to the magic numbers, spin and parity values of the ground state of the nucleus, but it is less successful in predicting magnetic moments. The collective model combines the features of the both models taking into account the interactions between valance nucleons and core that cause the deformation of the equilibrium shape of the nucleus [2-4].

The nuclear shape can be expressed by an expansion in spherical harmonics with time-dependent shape parameters. Deformed moving surface is described as below.

$$R(\theta,\phi,t) = R_0(1+\sum_{\lambda,\mu}\alpha_{\lambda,\mu}(t)Y_{\lambda,\mu}(\theta,\phi)) \qquad (2.1.1)$$

where R_0 is the radius in spherical equilibrium shape of the nucleus and $Y_{\lambda,\mu}(\theta,\phi)$ is the spherical harmonics. $\alpha_{\lambda,\mu}(t)$ are the expansion parameters depending on the time

and describes to surface deformations. Since the radius must be real, the description below is reached,

$$\alpha_{\lambda,\mu}(t) = (-1)\alpha^{*}_{\lambda,-\mu}(t) \tag{2.1.2}$$

When the coefficients $\alpha_{\lambda,\mu}(t)$ are small, the potential and kinetic energy have the forms below, respectively

$$V = \frac{1}{2}\sum_{\lambda,\mu} C_{\lambda} \left|\alpha_{\lambda,\mu}\right|^{2} \tag{2.1.3}$$

$$T = \frac{1}{2}\sum_{\lambda,\mu} B_{\lambda} \left|\dot{\alpha}_{\lambda,\mu}\right|^{2} \tag{2.1.4}$$

where C_{λ} and B_{λ} describe the properties of the nuclear matter. The Hamiltonian of the system is expressed in the classical form, as

$$H = T + V = \sum_{\lambda,\mu} \left(\frac{1}{2B_{\lambda}}\left|\pi_{\lambda,\mu}\right|^{2} + \frac{C_{\lambda}}{2}\left|\alpha_{\lambda,\mu}\right|^{2}\right) \tag{2.1.5}$$

with the frequencies

$$\omega_{\lambda} = \sqrt{\frac{C_{\lambda}}{B_{\lambda}}} \tag{2.1.6}$$

and the momentum conjugates are

$$\pi_{\lambda,\mu} = \frac{\partial T}{\partial \dot{\alpha}_{\lambda,\mu}} = B_{\lambda}\dot{\alpha}^{*}_{\lambda,\mu} \tag{2.1.7}$$

The most appropriate mode of them is $\lambda = 2$. In case of $\lambda = 0$, the spherical harmonics are constant and the situation corresponds only to the change of the radius of the nucleus. Because the nucleus can't be compressed, the mode isn't compatible with reality. Since the mode $\lambda = 1$ corresponds to shift of the center of mass, it is disregard of the nuclear excitations. The octupole deformations similar to shape of a pear, $\lambda = 3$, have negative parities. That's why it is not appropriate for studies on even-even nuclei. On the other hand, for hexadecupole deformation, $\lambda = 4$, any experimental evidence characterizing the nuclear spectrum isn't observed so far. The highest modes are of no practical-importance because of the limitations on λ. The "bumps" on the nuclear surface described the spherical harmonics decreases with increasing λ. It is easily seen that the bumps should not to be smaller than the radius of a nucleon. The condition leads us to the marginal results for higher modes.

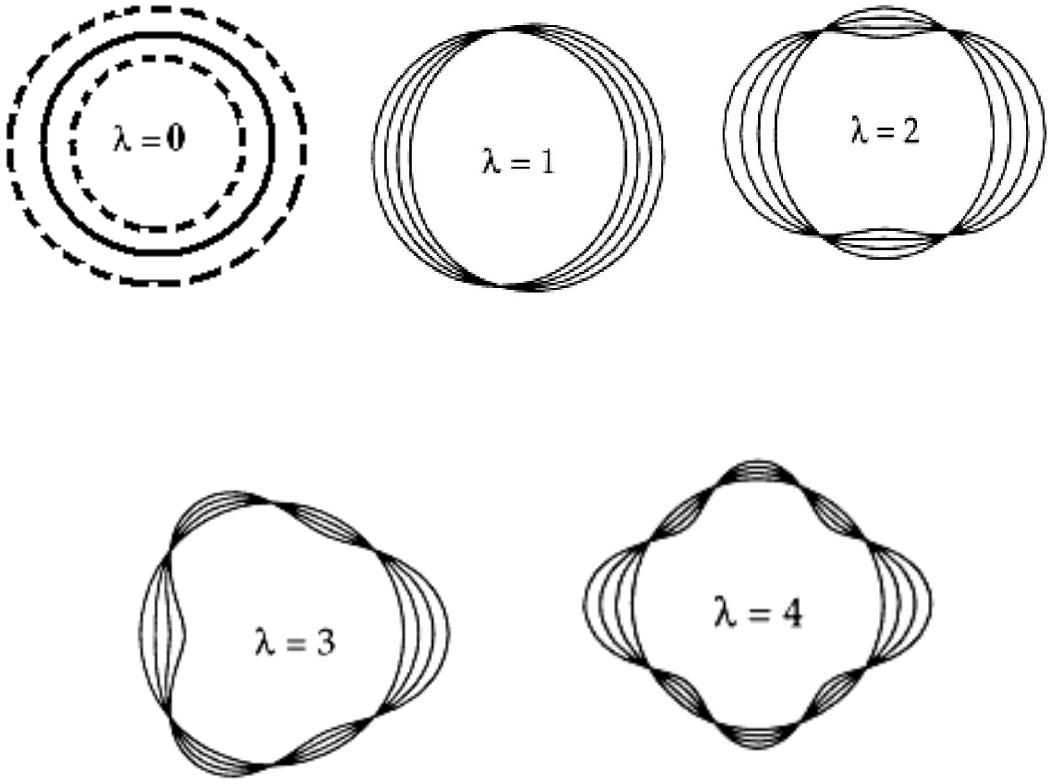

Figure 2.1: The different vibration modes depending on λ.

In the mode of $\lambda = 2$, using the Cartesian coordinates we obtain the forms of spherical harmonics.

$$x = \sin\theta\cos\phi \quad ; \quad y = \sin\theta\sin\phi \quad ; \quad z = \cos\theta \quad ; \quad x^2 + y^2 + z^2 = 1$$

$$Y_{2,\pm1}(\theta,\phi) = \mp\sqrt{\frac{15}{8\pi}}\sin\theta\cos\theta e^{\pm i\phi} = \mp\sqrt{\frac{15}{8\pi}}(xz \pm iyz)$$

$$Y_{2,0}(\theta,\phi) = \sqrt{\frac{15}{16\pi}}(3\cos^2\theta - 1) = \sqrt{\frac{15}{16\pi}}(2z^2 - x^2 - y^2)$$

$$Y_{2,\pm2}(\theta,\phi) = \sqrt{\frac{15}{32\pi}}\sin^2\theta e^{\pm 2i\phi} = \sqrt{\frac{15}{32\pi}}(x^2 - y^2 \pm 2ixy) \qquad (2.1.8)$$

The coefficients $\alpha_{2,\mu}$ are found in terms of the Cartesian deformation components as

$$R(x,y,z) = R_0(1 + \alpha_{xx}x^2 + 2\alpha_{xy}xy + \alpha_{yy}y^2 + 2\alpha_{yz}yz + \alpha_{zz}z^2 + 2\alpha_{zx}zx) \qquad (2.1.9)$$

$$\alpha_{2,\pm1} = \sqrt{\frac{8\pi}{15}}(\alpha_{xz} \pm i\alpha_{yz}) \quad ; \quad \alpha_{2,0} = \sqrt{\frac{8\pi}{90}}(2\alpha_{zz} - \alpha_{xx} - \alpha_{yy}) \quad ;$$

$$\alpha_{2,\pm2} = \sqrt{\frac{8\pi}{60}}(\alpha_{xx} - \alpha_{yy} \pm 2i\alpha_{xy})$$

At this stage, the orientation in space of the deformed nucleus should be clarified further. For this purpose, the principal axis system is used. Since the Cartesian deformation tensor must be diagonal, so that

$$\alpha'_{xy} = \alpha'_{yz} = \alpha'_{zx} = 0 \qquad (2.1.10)$$

The expressions below are obtained

$$\alpha'_{2,\pm1} = 0 \quad ; \quad \alpha'_{2,0} = \sqrt{\frac{8\pi}{90}}(2\alpha'_{zz} - \alpha'_{xx} - \alpha'_{yy}) \equiv a_0 \quad ; \quad \alpha'_{2,\pm2} = \sqrt{\frac{8\pi}{60}}(\alpha'_{xx} - \alpha'_{yy}) \equiv a_2 \tag{2.1.11}$$

- a_0 indicates the stretching of the z' with respect to x' and y' the axes,

- a_2 determines the difference in length between x' and y' axes,

-The three Euler angles $\theta = (\theta_1, \theta_2, \theta_3)$ determine the orientation of the principal axis system (x', y', z') with respect to laboratory-fixed frame (x, y, z).

Because the Euler angles characterize rotation of the nucleus without any change in the shape, the principal axis system is a convenient mathematical tool not only to describe rotation but also to separate the Hamiltonian into the parts of rotation and shape vibration.

A set of parameters introduced by Bohr and Mottelson is convenient to describe the deformation in terms of β.

$$a_0 = \beta\cos\gamma \qquad ; \qquad a_2 = \frac{1}{\sqrt{2}}\beta\sin\gamma \tag{2.1.12}$$

Then the deformation can be considered as below

$$\sum_{\mu}\left|\alpha_{2,\mu}\right|^2 = \sum_{\mu}\left|\alpha'_{2,\mu}\right|^2 = \beta^2 \tag{2.1.13}$$

In terms of spherical harmonics the radius is

$$R(\theta,\phi)=R_0\left[1+\beta\sqrt{\frac{5}{16\pi}}(\cos\gamma(3\cos^2\theta-1)+\sqrt{3}\sin\gamma\sin^2\theta\cos 2\phi)\right] \qquad (2.1.14)$$

The changes of the radius depending on β and γ in the principal axis system is given [22] as

$$\delta R_{x'}=R(\frac{\pi}{2},0)-R_0=R_0\sqrt{\frac{5}{4\pi}}\beta\cos(\gamma-\frac{2\pi}{3})$$

$$\delta R_{y'}=R(\frac{\pi}{2},\frac{\pi}{2})-R_0=R_0\sqrt{\frac{5}{4\pi}}\beta\cos(\gamma+\frac{2\pi}{3})$$

$$\delta R_{z'}=R(0,0)-R_0=R_0\sqrt{\frac{5}{4\pi}}\beta\cos\gamma \qquad (2.1.15)$$

Using a new notation δR_k, the three equations above can be exhibited in the form [23]

$$\delta R_k=R_0\sqrt{\frac{5}{4\pi}}\beta\cos(\gamma-\frac{2\pi k}{3}) \qquad (2.1.16)$$

The equation can be understood by Fig.2.2 where the dependence of Eq(2.1.16) on γ can be clearly seen. At the $\gamma=0$, the nucleus is elongated along the z' axis, while x' and y' axes are equal with each other, which is called prolate shape. For the $\gamma=\pi/3$, this time z' and x' axes are equal and longer than y', which is called oblate shape. The situation is repeated in each region of $\pi/3$ along 2π, only changing the axis it is directed. Therefore, in the region between $\gamma=0$ and $\gamma=\pi/3$ possible all the deformations are placed.

The kinetic energies of the system is given as below,

$$T_{vib} = \frac{1}{2} B(\dot{\beta}^2 + \beta^2 \dot{\gamma}^2) \tag{2.1.17}$$

$$T_{rot} = \frac{1}{2} \sum_{k=1}^{3} J_k \omega_k^2 \tag{2.1.18}$$

and moments of the inertia are

$$J_k = 4B\beta^2 \sin^2(\gamma - \frac{2\pi}{3} k) \quad . \tag{2.1.19}$$

Figure 2.2: a) Plot of the Eq.(2.1.16) , showing the change in length of the axes, x', y' and z'. **b)** The (β,γ) plane is divided into six equal parts. The part between 0^0 and 60^0 contains all shapes

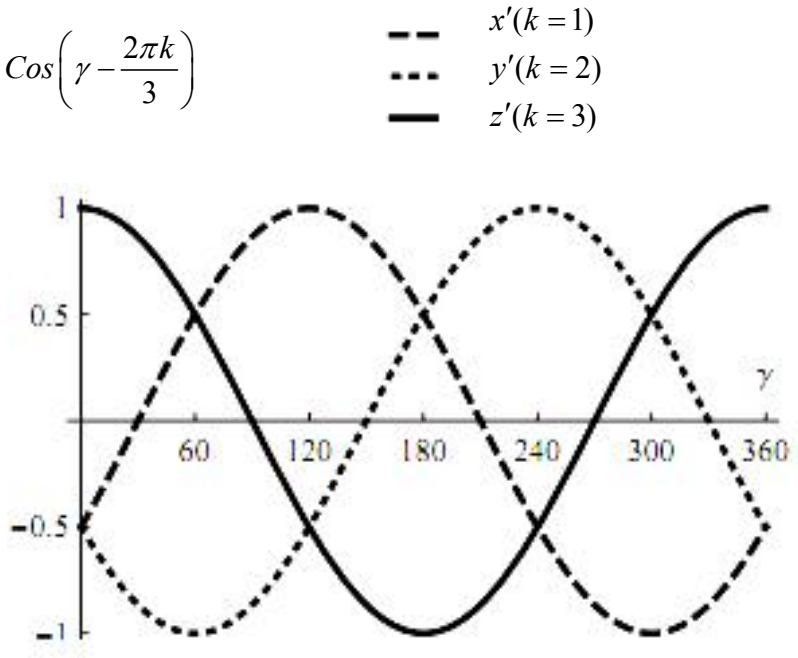

(a)

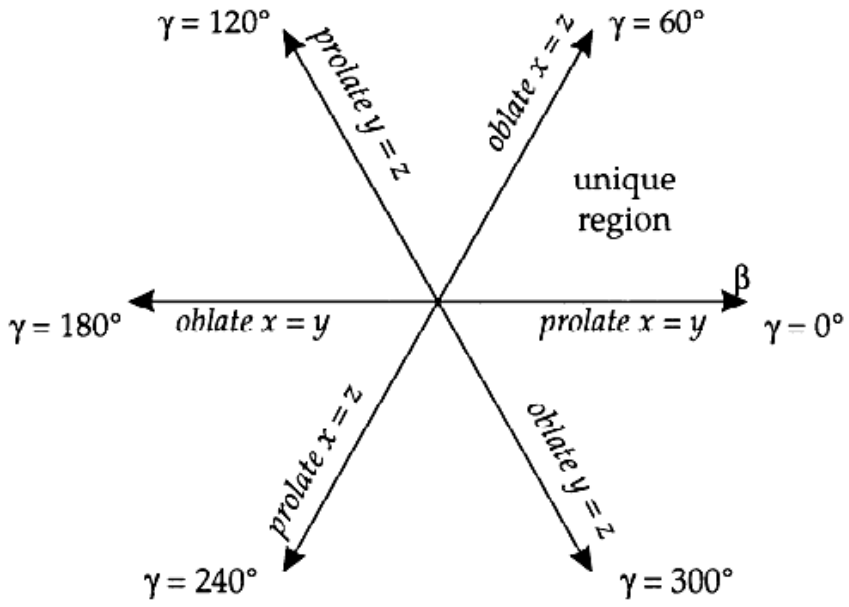

(b)

2.1.1 BOHR HAMILTONIAN

To constitute the Bohr Hamiltonian which describes the spectrum and wavefunction of the collective mode, firstly, we describe the Euler angles and the collective coordinates as

$$q_1 = \theta_1 \quad ; \quad q_2 = \theta_2 \quad ; \quad q_3 = \theta_3 \quad ; \quad q_4 = \beta \quad ; \quad q_5 = \gamma \tag{2.1.20}$$

The kinetic energy in the Bohr Hamiltonian is given as

$$T = \frac{B}{2}\left(\frac{ds}{dt}\right)^2 \tag{2.1.21}$$

where the square of the displacement is $ds^2 = g_{ij} dq_i dq_j$. The Hamiltonian can be obtained by means of the Pauli-Podolsky prescription as the manner of quantum mechanical [24].

$$\nabla^2 \Phi = \frac{1}{\sqrt{g}} \partial_i \sqrt{g} g^{ij} \partial_j \Phi \tag{2.1.22}$$

where the symmetric matrix is

$$g_{ij} = \begin{pmatrix} g_{11} & g_{12} & g_{13} & 0 & 0 \\ g_{21} & g_{22} & 0 & 0 & 0 \\ g_{31} & 0 & g_{33} & 0 & 0 \\ 0 & 0 & 0 & g_{44} & 0 \\ 0 & 0 & 0 & 0 & g_{55} \end{pmatrix} \tag{2.1.23}$$

g and g^{ij} are determinant and inverse matrix of the g_{ij}, respectively [25],

$$g = \frac{J_1 J_2 J_3}{B^3} \beta^2 \sin^2 \theta_2 = 4\beta^8 \sin^2 3\gamma \sin^2 \theta_2 \tag{2.1.24}$$

where moments of the inertia are

$$J_k = 4B\beta^2 \sin^2(\gamma - k\frac{2\pi}{3}) \tag{2.1.25}$$

Finally, from the Eq.(2.1.22) we have the Bohr Hamiltonian with any potential in terms of the collective variables as

$$H = -\frac{\hbar^2}{2B}\left[\frac{1}{\beta^4}\frac{\partial}{\partial\beta}\beta^4\frac{\partial}{\partial\beta} + \frac{1}{\beta^2 \sin 3\gamma}\frac{\partial}{\partial\gamma}\sin 3\gamma\frac{\partial}{\partial\gamma} - \frac{1}{4B^2}\sum_{k=1}^{3}\frac{\hat{Q}_k^2}{\sin^2(\gamma - \frac{2\pi}{3}k)}\right] + V(\beta,\gamma) \tag{2.1.26}$$

$\hat{Q}_k$ are the components of the angular momentum in the intrinsic frame.

$$\hat{Q}_1 = \hat{Q}_x = -i(-\frac{\cos\theta_3}{\sin\theta_2}\frac{\partial}{\partial\theta_1} + \sin\theta_3\frac{\partial}{\partial\theta_2} + \cot\theta_2\cos\theta_3\frac{\partial}{\partial\theta_3}),$$

$$\hat{Q}_2 = \hat{Q}_y = -i(-\frac{\sin\theta_3}{\sin\theta_2}\frac{\partial}{\partial\theta_1} + \cos\theta_3\frac{\partial}{\partial\theta_2} - \cot\theta_2\sin\theta_3\frac{\partial}{\partial\theta_3}),$$

$$\hat{Q}_3 = \hat{Q}_z = -i\frac{\partial}{\partial\theta_3} \tag{2.1.27}$$

The collective wavefunction is

$$\Psi(\beta,\gamma,\theta_i) = f(\beta)\Phi(\gamma,\theta_i) \tag{2.1.28}$$

$\Phi^{I,\tau}_{M,K}$ is given in terms of Wigner functions, $D^{I}_{M,K}(\theta_I)$ as

$$\Phi^{I,\tau}_{M,K}(\gamma,\theta_i) = \sqrt{\frac{2I+1}{16\pi^2(1+\delta_{K,0})}} g^{I,\tau}_{K}(\gamma)\left[D^{I}_{M,K}(\theta_I) + (-1)^I D^{I}_{M,-K}(\theta_I) \right] \tag{2.1.29}$$

where I is the quantum number of angular momentum, M and K are the projections of the quantum number I on laboratory-fixed frame and body-fixed frame, respectively, as seen in Fig.2.3.

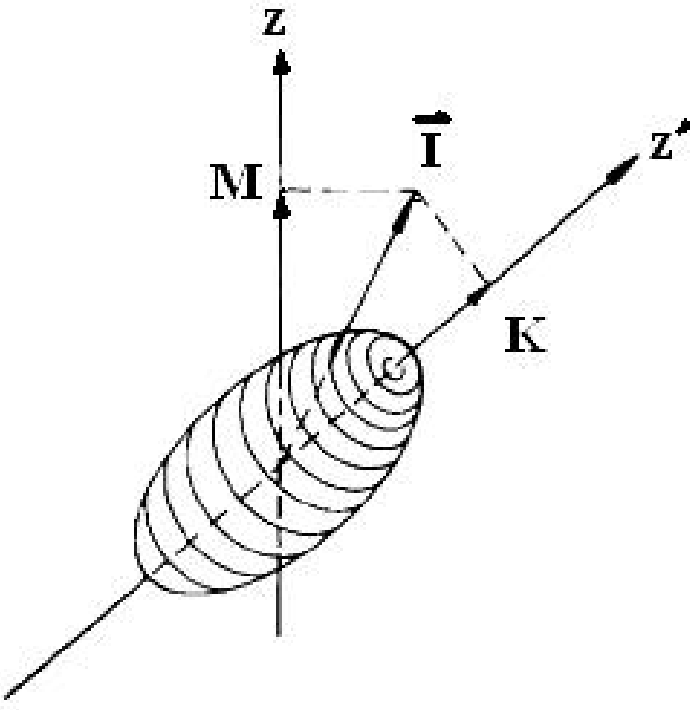

Figure 2.3: The projections of the total angular momentum vector on laboratory-fixed frame and body-fixed frame

The normalization condition and the volume element is given as

$$1=\int_{\beta=0}^{\infty}\int_{\gamma=0}^{\pi/3}\int_{\theta_1=0}^{2\pi}\int_{\theta_2=0}^{\pi}\int_{\theta_3=0}^{2\pi}\Psi^{*}(\beta,\gamma,\theta_1,\theta_2,\theta_3)\Psi(\beta,\gamma,\theta_1,\theta_2,\theta_3)dv \qquad (2.1.30)$$

$$dv=\beta^4 d\beta\left|\sin 3\gamma\right| d\gamma d\theta_1 \sin\theta_2 d\theta_2 d\theta_3 \qquad (2.1.31)$$

2.2 CRITICAL POINT SYMMETRIES

In the spectrum obtained by the Bohr Hamiltonian, the ratio $R_{4/2}$ is one of the most important arguments to describe the shape phase belonging to the nucleus in terms of collective dynamics. It represents ratio of the energies of the 4_1^+ level to the first exited state 2_1^+ as in the form

$$R_{4/2}=\frac{E(4_1^+)-E(0_1^+)}{E(2_1^+)-E(0_1^+)} \qquad (2.2.1)$$

In the frame of the collective model, $R_{4/2}=2.0;2.5;3.3$ corresponds to the spherical harmonic oscillator, γ-unstable rotor and axially symmetric prolate rotor, respectively.

-For $R_{4/2}=2.0$, the nuclei around the closed-shell have a nearly spherical shape and the surface vibrations.

-For $R_{4/2}=2.5$, the shape of nuclei continuously varies between prolate and oblate. Due to lack of a stable shape, the potential is independent of γ. At any time, the lengths of all three axes are different.

-For $R_{4/2}=3.3$, the nuclei having the number of nucleons far from the closed-shell configuration have permanently prolate or oblate deformed shape. In addition to vibration, they rotate perpendicular to symmetry axis.

These three limits constitute the edges of the Casten triangle in Fig.2.4 [26]. The shape phase transitions observed between the limits are the quantum phase

transitions depending on nucleon numbers as the control parameter, unlike usual phase transitions depending on continuous control parameters such as pressure, temperature, etc. The quantum phase transitions occur at the zero temperature and refer to, in practice, the changes in the equilibrium shape of the nucleus in the ground state without changing its energy.

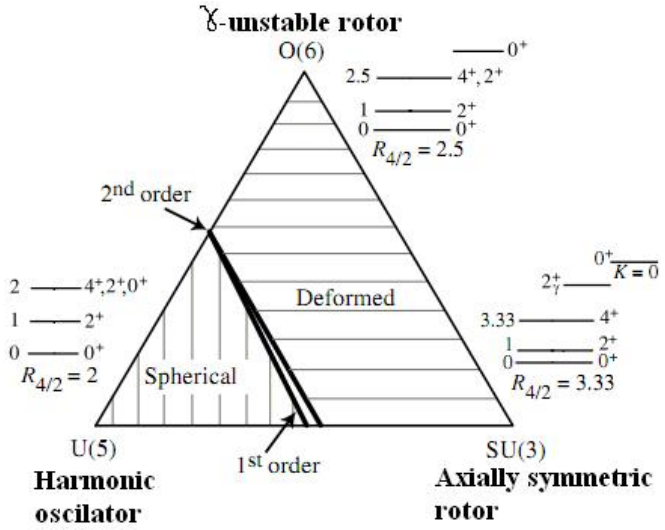

Figure 2. 4: The Casten triangle

2.2.1 E(5) CRITICAL POINT SYMMETRY

E(5) refers to a critical point where the transition from harmonic oscillator to γ-unstable rotor occurs. According to Ehrenfest classification, at the critical point the second order phase transition appears, because the second derivative of the order parameter according to the control parameter, nucleon number, is discontinuous, which is seen in Fig.2.5. The transition requires a flat minimum on the beta-dependent potential. On the other hand, throughout the region between harmonic oscillator and γ-unstable rotor, since the nuclei don't have a permanent deformation shape, the potential is independent of γ.

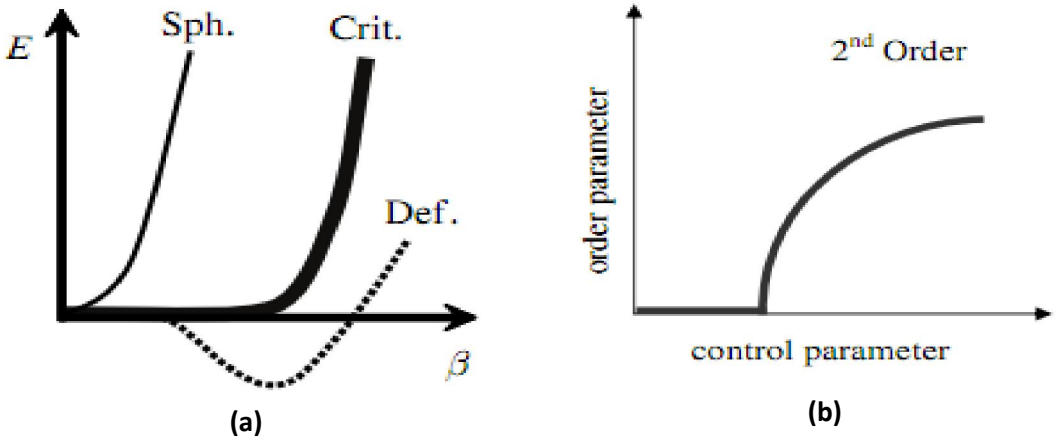

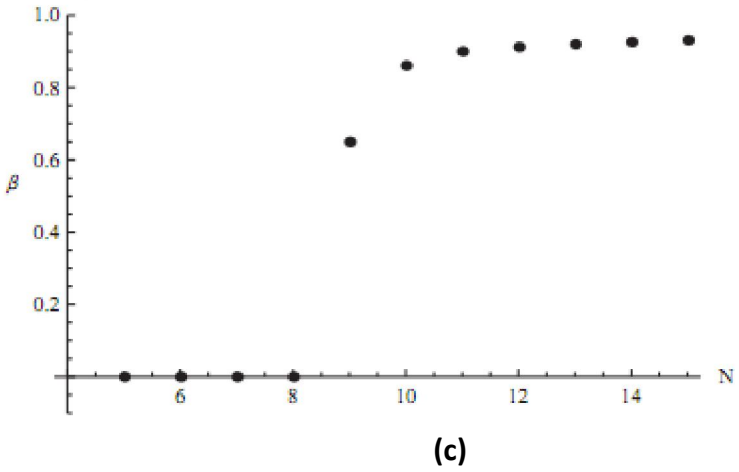

Figure 2. 5:
a) Energy surfaces respect to the deformation for the second order phase transition

b) Plot showing second order phase transition

c) Change of the deformation with respect to control parameter, nucleon number.

The analytical solutions of the E(5) critical point symmetry are obtained by means of the infinite well potential depending only on the variable β [5]. The solution leads us to $R_{4/2} = 2.2$ ratio.

2.2.2 X(5) CRITICAL POINT SYMMETRY

X(5) refers to a critical point where the transition from harmonic oscillator to axially symmetric prolate rotor occurs. According to Ehrenfest classification, at the critical point the first order phase transition appears, because the first derivative of the order parameter according to the control parameter is discontinuous, which is

seen in Fig.2.6. As seen the figure, at the point where the phase transition occurs there is a barrier and, as the result of that, the transition appears suddenly. $R_{4/2}$ ratio is 2.9 .

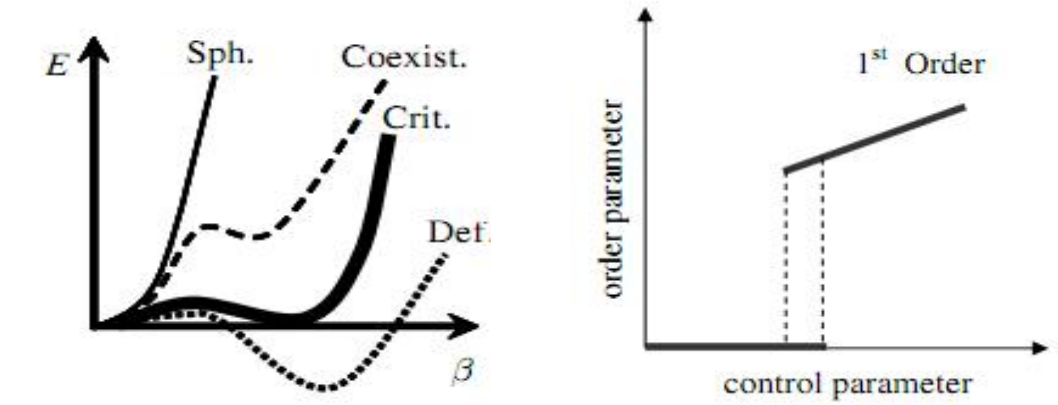

(a) (b)

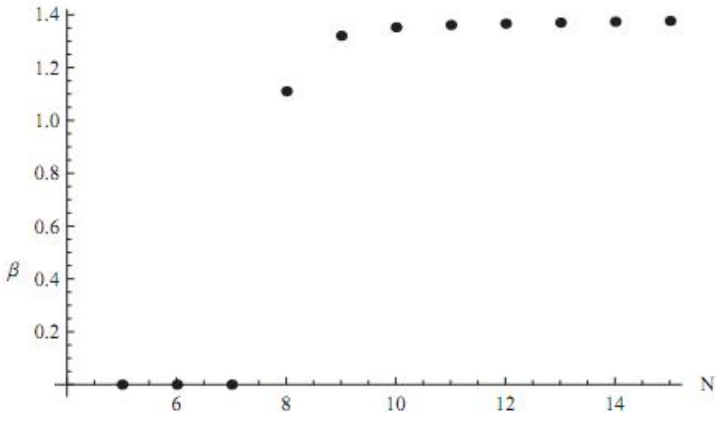

(c)

Figure 2.6:
a) Energy surfaces respect to the deformation for the first order phase transition

b) Plot showing first order phase transition

c) Change of the deformation with respect to control parameter, nucleon number.

2.3 DISCUSSION ON THE WOODS-SAXON POTENTIAL

For a theoretical background required for the next section, this section deals with the analytic solution of the W-S potential within the consideration of non-relativistic physics due to the structure of the Bohr Hamiltonian. To clarify first that the standard form of this potential is not exactly solvable for the angular momentum $l=0$, unlike some incorrect discussions in the literature [16-19], we start here with its extended form.

Since the standard well known form of the W-S potential does not derive single-particle levels with enough accuracy for a wide nucleic region, extended forms of this potential can be required in the most applications [20,27]. Especially, the simplest form [20] of these functions has been often studied [28-33]. The present analysis related to W-S potential is very important for the work presented here. To understand clearly the following discussion, we need to give a review of the related part in Ref. [20],

The closed form of the algebraic solutions for the modified spherically symmetric W-S potential,

$$V(r)=-\frac{V_0}{\left[e^{2a(r-R)}+1\right]}-\frac{We^{2a(r-R)}}{\left[e^{2a(r-R)}+1\right]^2} \tag{2.3.1}$$

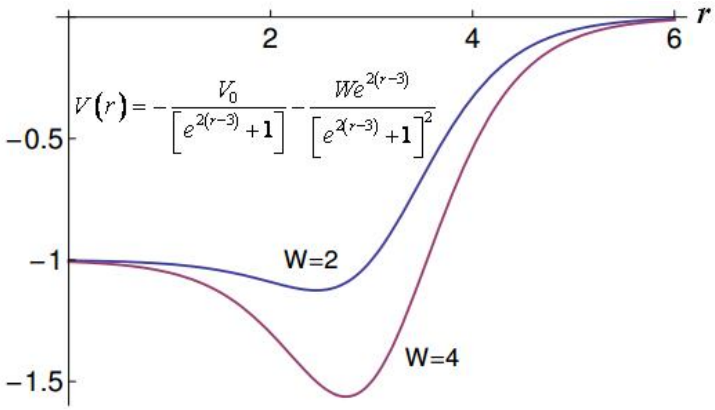

Figure 2.7: The Woods-Saxon potential with a dip near its surface is shown for special values of its free parameters, used for simplicity. All quantities shown are dimensionless.

are

$$E_n = -\frac{a^2}{4}\left\{\left[\sqrt{1+W/a^2}-(2n+1)\right]^2+\left[\frac{V_0/a^2}{\sqrt{1+W/a^2}-(2n+1)}\right]^2\right\}-\frac{V_0}{2} \quad (2.3.2)$$

and

$$\Psi_n(r) \propto \left[\frac{1}{e^{2a(r-R)}+1}\right]^{b/2}\left[1-\frac{1}{e^{2a(r-R)}+1}\right]^{c/2} P_n^{(b,c)} \quad (2.3.3)$$

In the above equations, $2a = 1/a_0$ with a_0 being the diffuseness parameter that determines the thickness of a surface layer in which the potential falls off from outside to its maximum strength inside a nucleus and R is the mean radius of the nucleus of interest where the average interaction takes place. The additional term with W in Eq. (2.3.1), which naturally arises in the calculations performed by [20], is responsible for modifying the standard well known W-S potential appeared as the first term in Eq. (2.3.1), providing the flexibility to construct the surface structure of the related nucleus. The corresponding wavefunction in Eq.(2.3.3) is expressed in terms of Jacobi polynomials, $P_n^{(b,c)}$, due to the technique used in Ref. [20], in which $b, c > -1$, as the real parameters in the polynomial considered, which serves as a testing ground for the reliability of the present calculations and $n = 0,1,2,\ldots$ being as the radial quantum number. The strengths of the potential in Eq.(2.3.1) can be expressed in the form of

$$V_0 = a^2\left(b^2-c^2\right) > 0 \quad , \quad W = a^2\left[(b+c)(b+c+4n+2)+4n(n+1)\right] > 0 \quad (2.3.4)$$

which is the milestone in the forthcoming discussion given below in justifying that there is no explicit expression for the eigenvalues of the usual W-S potential. After

some simple algebra, the orthogonal polynomial parameters gain physical meanings such that

$$b=\frac{1}{2}\left[\sqrt{1+W/a^2}-(2n+1)+\frac{V_0/a^2}{\sqrt{1+W/a^2}-(2n+1)}\right] \tag{2.3.5}$$

$$c=\frac{1}{2}\left[\sqrt{1+W/a^2}-(2n+1)-\frac{V_0/a^2}{\sqrt{1+W/a^2}-(2n+1)}\right] \tag{2.3.6}$$

which impose some constraints on the potential parameters and certainly determines the number of physically reasonable bound states for a deep potential appearing near the surface as will be clear below in this section.

At this stage, we are in a position to make an exciting connection between the attractive potential in Eq.(2.3.1) and the familiar effective W-S potential including the repulsive barrier term ($\hbar=2m=1$),

$$U_{eff}(r)=-\frac{U_0}{\left[e^{(r-R)/a_0}+1\right]}+\frac{\ell(\ell+1)}{r^2} \tag{2.3.7}$$

which cannot be exactly solved. Nevertheless, the recent works in [16-19, 21] have employed the widely used Pekeris approximation [14] in their calculations. Firstly, the barrier term is expanded in the Taylor Series around the point $x\approx 0$.

$$\frac{\ell(\ell+1)}{r^2}=\frac{\ell(\ell+1)}{R^2}\frac{1}{(1+x)^2}=\delta(1-2x+3x^2-4x^3+...) \tag{2.3.8}$$

$$x=\frac{r-R}{R}, \qquad r=R(1+x), \qquad \delta=\frac{l(l+1)}{R^2}$$

Considering the Pekeris Approximation, we shall replace the barrier term by the expression below

$$\frac{\ell(\ell+1)}{r^2} \simeq \delta\left(C_0 + \frac{C_1}{e^{(r-R)/a_0}+1} + \frac{C_2}{\left(e^{(r-R)/a_0}+1\right)^2} \right) \tag{2.3.9}$$

To obtain the constants, we again expand the right side of the equation in the Taylor Series around the point $x \approx 0$.

$$\frac{\ell(\ell+1)}{r^2} \simeq \delta\left((C_0 + \frac{C_1}{2} + \frac{C_2}{4}) - \frac{R}{4a_0}(C_1 + C_2)x + \frac{R^2}{16a_0^2}C_2x^2 + ... \right) \tag{2.3.10}$$

Comparing equal powers of x, we obtain the constants as

$$C_0 = 1 - \frac{4a_0}{R} + \frac{12a_0^2}{R^2} \quad , \quad C_1 = \frac{8a_0}{R} - \frac{48a_0^2}{R^2} \quad , \quad C_2 = \frac{48a_0^2}{R^2} \tag{2.3.11}$$

Although this approach is valid only for low vibrational states, such a treatment does not cause any physical problem in our application in the next section, because this set of states contains the most important low-lying levels necessary to characterize the collective excitations of the nucleus within the scheme of the Bohr Hamiltonian. Hence, the full potential in Eq.(2.3.7) is safely approximated to

$$U_{eff}(r) \simeq \delta C_0 - \frac{(U_0 - \delta C_1)}{\left[e^{(r-R)/a_0}+1\right]} + \frac{\delta C_2}{\left[e^{(r-R)/a_0}+1\right]^2} \tag{2.3.12}$$

which, in its present form, yields algebraic closed solutions. Note that δC_0 constant in Eq.(2.3.12) will be later invoked into the corresponding energy value. To observe the close relation between the equation above and Eq.(2.3.1), we remind that $\frac{e^{2a(r-R)}}{\left[e^{2a(r-R)}+1\right]^2}=\frac{1}{e^{2a(r-R)}+1}-\frac{1}{\left[e^{2a(r-R)}+1\right]^2}$, therefore Eq. (2.3.1) can easily be transformed to

$$V(r)=-\frac{\left(V_0+W\right)}{\left[e^{2a(r-R)}+1\right]}+\frac{W}{\left[e^{2a(r-R)}+1\right]^2} \tag{2.3.13}$$

From the comparison of Eqs. (2.3.12) and (2.3.13) it is obvious that

$$W=\delta C_2=\frac{12\ell\left(\ell+1\right)}{a^2R^4} \quad , \quad V_0=U_0-\frac{4\ell\left(\ell+1\right)}{aR^3} \tag{2.3.14}$$

as $a_0=1/2a$ mentioned above. This simple analysis, unlike the previous works in Refs. [16-19], justifies clearly that both potential given by Eqs. (2.3.1) and (2.3.7) do not admit an analytical solution in case $\ell=0$ due to the additional strength in the potentials $\left(W=0\right)$ denoted by Eq.(2.3.14) that leads to unphysical polynomial parameters $\left(b,c\right)$ in Eqs.(2.3.5) and (2.3.6) which should in fact satisfy $b,c>-1$ condition because of the mathematical definition of Jacobi polynomials. Additionally, from Eq.(2.3.4), $b+c=\left[\sqrt{1+W/a^2}-\left(2n+1\right)\right]>0$ that restricts the the strengths of the physically acceptable potential parameters, especially for $\ell=0$, as

$$0\le n<\frac{\sqrt{1+12\frac{\ell\left(\ell+1\right)}{a^4R^4}}-1}{2} \tag{2.3.15}$$

in connection with the physically meaningful bound states exist in the system of interest. The reader is referred to Ref. [20] for a more comprehensive discussion. A similar exhaustive discussion on the same topic may be found in [21].

To close this brief but necessary discussion, we go back to the solutions, Eqs. (2.3.2) and (2.3.3), of the modified W-S potential in Eq.(2.3.1) and bearing in mind the discussion above together in particular with the comparison results in (2.3.14), the replacement of the required terms reproduces explicitly the energy expression for the W-S potential in Eq.(2.3.12).

$$\varepsilon_n = \frac{\ell(\ell+1)}{R^2}\left(1+\frac{12a_0^2}{R^2}\right) - \left[\frac{\sqrt{1+\left(192\ell(\ell+1)a_0^4/R^4\right)}-(2n+1)}{4a_0}\right]^2 - \left[\frac{U_0 a_0 - 8\ell(\ell+1)a_0^2/R^3}{\sqrt{1+\left(192\ell(\ell+1)a_0^4/R^4\right)}-(2n+1)}\right]^2 - \frac{U_0}{2} \tag{2.3.16}$$

which is identical to the corresponding result obtained by [21]. The related wavefunction can be readily expressed, if necessary, in the same manner considering Eqs. (2.3.3), (2.3.5), (2.3.6) and (2.3.14) all together.

We finally remark that the calculations required in the following section will be carried out in five dimensions as Eq.(2.3.12) cannot be solved analytically in three dimensions for $\ell = 0$ case because of the constraints mentioned above, in spite of the mathematical possibility in Eq. (2.3.16), which does not cause any physical problem due to the convenient structure of the Bohr Hamiltonian that needs to be considered in five dimensions. Therefore, the angular momentum (ℓ) appeared in the energy expressions above should be transformed to

$$\ell_N = \ell + \frac{N-3}{2} \tag{2.3.17}$$

in $N-$dimensional consideration [21,34].

CHAPTER 3

APPLICATIONS OF WOODS-SAXON POTENTIAL FOR THE BOHR HAMILTONIAN

3.1 APPLICATION OF WOODS-SAXON POTENTIAL FOR THE $\gamma-$ UNSTABLE CASE

This section focuses on the analytic solution of the Bohr Hamiltonian with the Woods-Saxon potential for the $\gamma-$unstable case. Great interest has been recently raised [7-12 and the references therein] by the analytical solution of $\gamma-$unstable collective Bohr Hamiltonian in case of exactly solvable quantum potentials in the β variable to describe the shape phase transition between spherical and $\gamma-$unstable nuclei. This situation provides us a testing ground to check the applicability and success of the specifically chosen algebraically solvable potential of interest here, which has been discussed in the preceding section, in theoretical analysis of atomic nuclei.

Starting with the Bohr Hamiltonian in Eq. (2.1.26) [2-4], and bearing in mind $\hbar^2=2M=1$ due to the discussion presented above, where β and γ are the usual collective coordinates describing the deformation and the shape of the nuclear surface, respectively, together with $\hat{Q}_\kappa\left(\kappa=1,2,3\right)$ being the components of the angular momentum, and considering the $\gamma-$independent potential case, $V\left(\beta,\gamma\right)=U\left(\beta\right)$, which allows the separation of variables as $\Psi\left(\beta,\gamma,\theta_i\right)=\beta^{-2}\phi\left(\beta\right)\Phi\left(\gamma,\theta_i\right)$, one arrives at the Schrödinger-like equation, in which l is replaced by τ in five dimension, that determines the spectrum of the entire collective system [5,12].

$$-\frac{d^2\phi}{d\beta^2}+\left[U(\beta)+\frac{(\tau+1)(\tau+2)}{\beta^2}\right]\phi(\beta)=\varepsilon_{n,\tau}\,\phi(\beta) \tag{3.1.1}$$

in which τ is the seniority quantum number taking the values $\tau=0,1,2,3,...$ [35]. The angular momentum L is given as in the form below

$$\tau=3\nu_\Delta+\mu\,,\quad ;\ \nu_\Delta=0,1,2....\ ;L=\mu,\mu+1,.....,2\mu-2,2\mu \tag{3.1.2}$$

where $2\mu-1$ is missing and ν_Δ is called as the missing quantum number[36]. The corresponding energy spectrum in Eq.(3.1.1) for the consideration of the Woods-Saxon like potential in Eq.(2.3.7), substituting r,R,a by β,β_0,a_0,respectively, can be expressed as

$$\varepsilon_{n,\tau}^{W-S}=\frac{(\tau+1)(\tau+2)}{\beta_0^2}\left(1+\frac{12a_0^2}{\beta_0^2}\right)-\left\{\frac{\sqrt{1+\left[192(\tau+1)(\tau+2)a_0^4/\beta_0^4\right]}-(2n+1)}{4a_0}\right\}^2-$$
$$\left\{\frac{U_0a_0-8(\tau+1)(\tau+2)a_0^2/\beta_0^3}{\sqrt{1+\left[192(\tau+1)(\tau+2)a_0^4/\beta_0^4\right]}-(2n+1)}\right\}^2-\frac{U_0}{2} \tag{3.1.3}$$

using the spirit of Eq. (2.3.14). To estimate the best values for the three parameters above (a_0, β_0 and U_0), one needs to consider the constraints introduced above, Eqs. (2.3.4), (2.3.5), (2.3.6),(2.3.12).(2.3.13) and particularly (2.3.15).

$$0\le n<\frac{\sqrt{1+192\dfrac{{a_0}^4(\tau+1)(\tau+2)}{\beta_0^4}}-1}{2} \tag{3.1.4}$$

Due to the interesting mathematical constraint above, only the lowest bandheads and energy spacings could be computed in the case of $n=0$. Taking the advantage of degenerations in the ground state, the bandheads and energy spacing belonging to the ground state and γ bands are successfully derived, which are obviously illustrated by Table (3.1). To show also explicitly the agreement between the findings obtained by our formalism and the related experimental data, the quality measure below is used that justifies the reliability of our theoretical results shown through Table (3.1).

$$\sigma=\sqrt{\frac{\sum_{i=1}^{N}(E_i(\exp)-E_i(th))^2}{(N-1)E(2_1^+)}} \tag{3.1.5}$$

As a first consideration along this line, Eq. (2.3.14) implies that if V_0 is a constant then U_0 depends on ℓ, and vice versa. We are going to consider here V_0 as being the constant quantity. Then we can use

$$U_0=V_0+\frac{8a_0(\tau+1)(\tau+2)}{\beta_0^3} \tag{3.1.6}$$

in order to eliminate U_0 from Eq. (3.1.3). Using the notation $A=a_0/\beta_0$,

$$\varepsilon_{n,\tau}^{W-S}=\frac{(\tau+1)(\tau+2)}{\beta_0^2}\left(1+12A^2-4A\right)-\left\{\frac{\sqrt{1+192(\tau+1)(\tau+2)A^4}-(2n+1)}{4a_0}\right\}^2-\left\{\frac{V_0\,a_0}{\sqrt{1+192(\tau+1)(\tau+2)A^4}-(2n+1)}\right\}^2-\frac{V_0}{2} \tag{3.1.7}$$

which has a similar form as in (2.3.2). Because of Iachello's works [5,6] on E(5) and X(5), people fit spectra leaving out overall scales, in order to reduce the number of parameters. The researchers do not fit the raw experimental levels E_L, but the quantities

$$\left(E_L - E_0\right)/\left(E_2 - E_0\right) \tag{3.1.8}$$

In other words, they subtract from all levels the energy of the ground state, and then they divide by the energy of the first excited state, which in even-even nuclei is the energy of the first excited state with $L = 2$. In the present case this has the following consequences on Eq. (3.1.7): (i) The last term, $-V_0/2$, plays no role since it is a constant and cancels out. (ii) Using the rescaling

$$\beta_0 = \frac{\tilde{\beta}_0}{\sqrt{V_0}} \quad , \quad a_0 = \frac{\tilde{a}_0}{\sqrt{V_0}} \tag{3.1.9}$$

a common factor V_0 appears in all terms of Eq. (3.1.7), which therefore cancels out when Eq. (3.1.8) above is used. (iii) Using $A = a_0/\beta_0 = \tilde{a}_0/\tilde{\beta}_0$, a common factor $\tilde{\beta}_0^2$ can be taken away from the denominator of all terms of (3.1.7). $\tilde{\beta}_0$ is related to the "well size", while A is related to the ratio of the diffuseness parameter over the average width of the potential. Then the equation to be used for the energy fits becomes

$$\varepsilon_{n,\tau}^{W-S} = \left(\tau+1\right)\left(\tau+2\right)\left(1+12A^2-4A\right) - \left\{\frac{\sqrt{1+192\left(\tau+1\right)\left(\tau+2\right)A^4}-\left(2n+1\right)}{4A}\right\}^2 - \left\{\frac{A\tilde{\beta}_0^2}{\sqrt{1+192\left(\tau+1\right)\left(\tau+2\right)A^4}-\left(2n+1\right)}\right\}^2 \tag{3.1.10}$$

This is the equation used in the fits, from which the parameters A and $\tilde{\beta}_0$ can be determined. Then $\tilde{a}_0$ is readily calculated from $\tilde{a}_0 = A\tilde{\beta}_0$. The Woods-Saxon potential is essentially active within its radius, *R*, which in this case is β_0. One way to fix the scale is to identify the radius of the potential, β_0, with the β_{exp} value obtained from the experimental values of $B\left(E2;0_1^+ \to 2_1^+\right)$ [37]. Then from Eq.(3.1.9) one simply has

$$V_0 = \frac{\tilde{\beta}_0^2}{\beta_{\text{exp}}^2} \tag{3.1.11}$$

Notice that in this case a_0 is calculated directly from $a_0 = A\beta_{\text{exp}}$. The ground state band has $n = 0$ and levels $L_g = 0,2,4,6,...,$ for which $\tau = L/2$. Thus within these bands one has

$$(\tau+1)(\tau+2) = (L+2)(L+4)/4 \tag{3.1.12}$$

Additionally, the $\gamma_1 -$band has $n = 0$ and levels with $L_\gamma = 2,3,4,5,...,$ which exhibit the following degeneracies:

$$2_\gamma = 4_g, \quad 3_\gamma = 4_\gamma = 6_g, \quad 5_\gamma = 6_\gamma = 8_g, \quad 7_\gamma = 8_\gamma = 10_g, ... \tag{3.1.13}$$

while $\beta_1 -$band has levels $L_\beta = 0,2,4,6,...$ having two choices: (i) $n = 0$, in which the following degeneracies hold

$$0_\beta = 6_g, \quad 2_\beta = 8_g, \quad 4_\beta = 10_g, \quad 6_\beta = 12_g, ... \tag{3.1.14}$$

(ii) $n = 1$. Then no degeneracies of this kind occur.

Table 3.1 Comparison of theoretical predictions of the Bohr Hamiltonian with the Woods-Saxon potential for $\gamma-$ unstable nuclei to experimental data [38] of rare earth and actinides with $R_{4/2} < 2.6$ and known 2^+_γ states. The angular momenta of the highest levels of the ground state and quasi-γ bands included in the rms fit are labelled by L_g and L_γ respectively, while N indicates the total number of levels involved in the fit and σ is the quality measure of Eq. (3.1.5). All energies are normalized to the energy of the first excited state, $E(2^+_1)$. For each band, the $R_{4/2} = E(4^+_1)/E(2^+_1)$ ratio (labelled by $4/2$, the normalized bandhead of the quasi-γ band (labelled as $2_\gamma/2$), and the normalized last members of the ground state and quasi-γ_1 bands included in the fit (labelled by $L_g/2$ and $L_\gamma/2$ respectively),are reported. The theoretical predictions are obtained from the Eq.(3.1.3).

Nucleus	$\tilde{\beta}_0$	$\tilde{A}$	$10^3\tilde{a}_0$	β_0	V_0	$10^3 a_0$	L_g	L_γ	N	σ	4/2 exp	4/2 th	$L_g/2$ exp	$L_g/2$ th	$2_\gamma/2$ exp	$2_\gamma/2$ th	$L_\gamma/2$ exp	$L_\gamma/2$ th
^{98}Ru	0.50	0.24	120	0.195	6.5	47	24	4	14	0.29	2.14	2.12	16.6	16.5	2.2	2.1	3.5	3.3
^{100}Ru	0.32	0.22	70	0.215	2.2	47	24	4	14	0.37	2.27	2.21	21.8	22.0	2.5	2.2	3.8	3.6
^{102}Ru	0.75	0.20	148	0.240	9.8	47	10	5	8	0.36	2.33	2.21	7.2	7.1	2.3	2.2	4.7	5.3
^{102}Pd	0.48	0.21	101	0.196	6.0	41	26	4	15	0.24	2.29	2.24	27.7	27.5	2.8	2.2	4.1	3.7
^{104}Pd	0.57	0.13	74	0.209	7.5	27	8	4	6	0.28	2.38	2.22	5.8	5.7	2.4	2.2	3.7	3.8
^{106}Pd	0.31	0.22	66	0.229	1.8	49	8	5	7	0.46	2.40	2.23	5.8	5.2	2.2	2.2	4.6	5.2
^{108}Pd	0.63	0.19	119	0.243	6.8	46	12	4	8	0.34	2.42	2.27	9.6	9.7	2.1	2.3	3.7	3.8
^{110}Pd	0.51	0.12	62	0.257	3.9	31	12	4	8	0.32	2.46	2.26	10.8	10.9	2.2	2.3	3.7	3.9
^{112}Pd	0.23	0.20	46	0.220	1.1	44	6	3	4	0.56	2.53	2.29	4.4	3.8	2.1	2.3	3.1	3.8
^{114}Pd	0.61	0.17	106	0.164	13.9	28	12	8	12	0.63	2.56	2.30	10.4	10.3	2.1	2.3	8.0	7.9
^{116}Pd	0.55	0.16	87	0.207	7.1	33	12	8	12	0.64	2.58	2.33	10.8	10.8	2.2	2.3	8.3	8.3
^{108}Cd	0.78	0.23	180	0.175	19.6	41	24	5	15	0.54	2.38	2.12	18.8	18.1	2.5	2.1	4.1	4.7
^{112}Cd	0.25	0.24	61	0.186	1.8	45	12	10	14	0.30	2.29	2.10	7.4	7.0	2.1	2.1	6.9	7.0

Table 3.1. (continued)

Nucleus	$\tilde{\beta}_0$	$\tilde{A}$	$10^3\tilde{a}_0$	β_0	V_0	$10^3 a_0$	L_g	L_γ	N	σ	4/2 exp	4/2 th	$L_g/2$ exp	$L_g/2$ th	$2_\gamma/2$ exp	$2_\gamma/2$ th	$L_\gamma/2$ exp	$L_\gamma/2$ th
^{114}Cd	0.22	0.22	49	0.190	1.4	42	6	2	3	0.07	2.30	2.21	3.6	3.6	2.2	2.2	2.2	2.2
^{118}Xe	0.13	0.18	23	0.265	0.2	48	14	8	13	0.26	2.40	2.34	12.9	13.1	2.8	2.3	7.8	8.0
^{120}Xe	0.21	0.17	36	0.291	0.5	50	14	9	14	0.47	2.47	2.37	13.8	13.6	2.7	2.4	9.8	10.8
^{122}Xe	0.52	0.14	71	0.259	4.0	35	16	9	15	0.65	2.50	2.32	17.5	17.6	2.5	2.3	9.7	11.1
^{124}Xe	0.57	0.16	88	0.212	7.2	33	12	8	12	0.51	2.48	2.32	11.0	10.8	2.4	2.3	8.2	8.2
^{126}Xe	0.65	0.18	115	0.188	11.9	33	12	9	13	0.63	2.42	2.28	11.0	10.1	2.3	2.3	9.1	10.1
^{128}Xe	0.67	0.21	143	0.184	13.4	39	10	7	10	0.47	2.33	2.20	7.6	6.9	2.2	2.2	6.2	6.9
^{130}Xe	0.92	0.22	203	0.169	29.4	37	14	5	10	0.30	2.25	2.11	9.5	9.5	2.1	2.1	4.1	4.7
^{132}Xe	0.90	0.24	218	0.141	41.2	34	6	2	3	0.34	2.16	2.05	3.2	3.2	1.9	2.1	1.9	2.1
^{134}Xe	1.10	0.27	302	0.119	85.6	33	8	5	7	0.29	2.04	1.82	3.5	3.1	1.9	1.8	2.7	3.1
^{130}Ba	0.31	0.09	28	0.218	2.0	20	12	6	10	0.35	2.52	2.33	11.8	11.9	2.5	2.3	5.9	6.3
^{132}Ba	0.66	0.13	85	0.186	12.5	24	14	8	13	0.57	2.43	2.10	12.1	12.0	2.2	2.1	6.2	7.2
^{134}Ba	1.04	0.20	208	0.161	41.8	32	8	4	6	0.33	2.32	2.05	4.7	4.6	1.9	2.0	3.3	3.3
^{134}Ce	0.16	0.19	30	0.195	0.7	37	12	8	12	0.71	2.56	2.32	10.2	10.2	2.4	2.3	7.4	7.9
^{138}Ce	1.09	0.25	276	0.126	74.8	32	14	2	7	0.21	2.32	1.94	6.7	6.6	1.9	1.9	1.9	1.9
^{142}Gd	0.75	0.18	137				8	2	4	0.23	2.35	2.22	5.4	5.4	1.9	2.2	1.9	2.2
^{156}Er	0.56	0.20	110	0.189	8.8	37	12	5	9	0.31	2.32	2.27	9.6	9.6	2.7	2.3	4.8	5.5
^{186}Pt	0.14	0.16	22	0.198	0.5	32	26	4	15	0.61	2.56	2.40	38.7	38.8	3.2	2.4	5.2	4.2
^{188}Pt	0.40	0.13	53	0.186	4.7	25	12	4	8	0.33	2.53	2.40	11.7	11.9	2.3	2.4	4.1	4.2
^{190}Pt	0.37	0.09	34	0.149	6.2	14	8	6	8	0.56	2.49	2.20	6.5	5.7	2.0	2.2	5.9	5.7

Table 3.1. (continued)

Nucleus	$\tilde{\beta}_0$	$\tilde{A}$	$10^3\tilde{a}_0$	β_0	V_0	$10^3 a_0$	L_g	L_γ	N	σ	4/2 exp	4/2 th	$L_g/2$ exp	$L_g/2$ th	$2_\gamma/2$ exp	$2_\gamma/2$ th	$L_\gamma/2$ exp	$L_\gamma/2$ th
^{192}Pt	0.49	0.11	54	0.153	10.2	17	10	8	11	0.69	2.48	2.19	8.6	7.8	1.9	2.2	8.2	7.8
^{194}Pt	0.45	0.14	62	0.143	10.0	20	10	2	5	0.27	2.47	2.37	8.7	8.8	1.9	2.4	1.9	2.4
^{196}Pt	0.44	0.15	67	0.130	11.6	20	10	2	5	0.25	2.47	2.38	8.6	8.6	1.9	2.4	1.9	2.4
^{198}Pt	0.74	0.15	113	0.114	42.1	17	6	4	5	0.45	2.42	2.16	4.2	3.6	1.9	2.2	3.5	3.6
^{200}Pt	0.71	0.24	169				4	2	2	0.36	2.35	2.10	2.3	2.1	1.8	2.1	1.8	2.1

The parameters obtained from the fitting procedure are fairly suitable and physically meaningful. The well depth V_0 exhibits a tendency to approach a minimum in the regions far from the closed-shells where the maximum deformation occurs as exhibited by $\beta_0 \equiv \beta_{\exp}$ [37] for a variety of nuclei. On the other hand, in the standard Woods-Saxon potential the diffuseness parameter is $a_0 = 0.67\,fm$, while the width of the potential, namely the radius of nuclei, is $R_0 = r_0 A^{1/3}$, where A is the mass number of the nucleus and $r_0 = 1.27\,fm$ [22]. As seen in the Table (3.1), for the most nuclei the ratio a_0 / R_0 is moderately close to the ratio of the standard W-S potential, which means that our model introduced in this report is physically reliable. As is clear from the table above, the related β_0 experimental values for a few nuclei are not available in Ref.[37], thus the necessary fixing procedure couldn't be performed for them. This exceptional situation, however, does not cause any physical problem when considering the whole of the applications.

To test the applicability of the Woods-Saxon potential in the description of nuclear spectra, we have first considered the *Xe*-isotopes as they show a nice transition from spherical to gamma unstable behaviour. Gaining confidence from these initial search, we have extended the scenario and fitted all nuclei with mass $A \geq 100$ and $R_{4/2} = E(4)/E(2) < 2.6$. The Woods-Saxon potentials obtained for the ${}_{54}Xe$ isotopes are shown in Fig.3.1.

As said before, in the standard Woods-Saxon potential, the ratio of a_0 / R_0 is moderately close to one of Xe series in which it is expressed by the parameter $A = a_0 / \beta_0 = \tilde{a}_0 / \tilde{\beta}_0$. As one moves from ${}^{134}Xe_{80}$, which is just below the $N = 82$ magic number, to the midshell nucleus ${}^{120}Xe_{66}$, the $\beta_0 \equiv \beta_{\exp}$ parameter increases as shown in Table (3.1), as well as reducing the well depth V_0. The reader is referred to Eq. (A3) in Appendix A to see the relation between β_0 and the minimum value $(\beta_{\min})$ of the potential. In addition, it seen that the slopes smoothly decreases when approaching the mid-shell region.

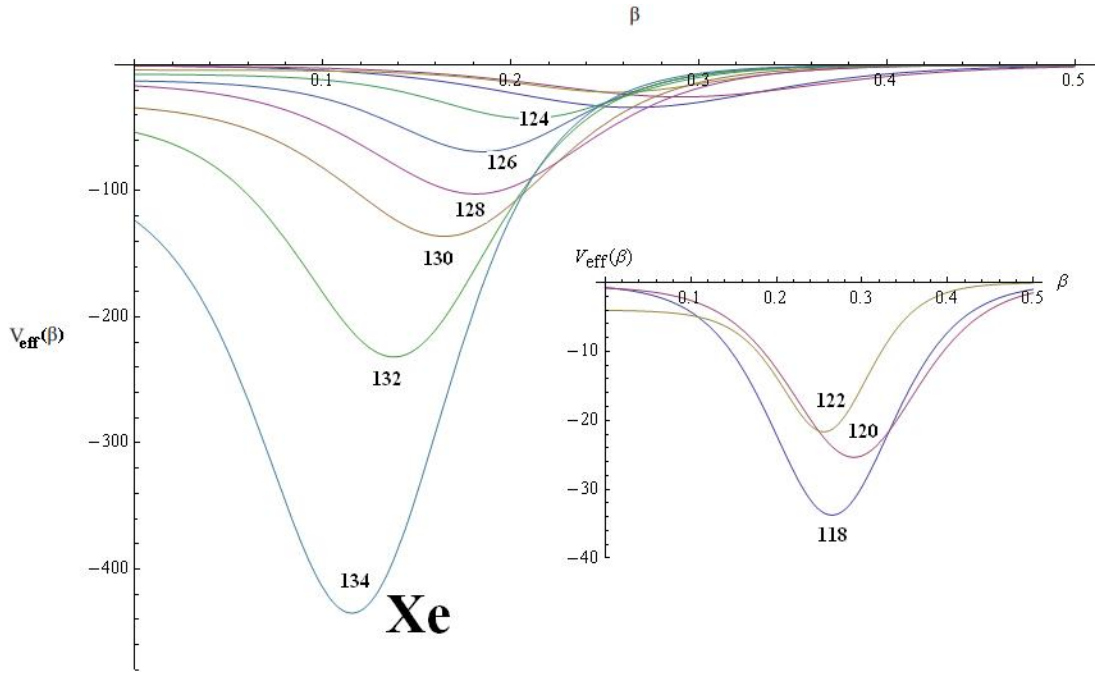

Figure 3. 1: Behaviour of the Woods-Saxon potentials used for the ${}_{54}Xe$ isotopes for an arbitrary $\tau(=1)$ value.

As a result, one gradually obtains in general less steep potentials with a minimum farther away from the origin. The trends start to be reversed with ${}^{120}Xe_{66}$. Further, as we go away from the closed shell and deeper into the *N*=50-82 shell, we get more collective *Xe* isotopes. Indeed, the 4_g value (also called the $R_{4/2}$ ratio) is increasing.

Although we have got fits and physical parameters of good quality up to now, one also must to take into account the accuracy of the Pekeris approximation. In the other words, it should also be investigated that how much the approximate potential used is similar to the exact potential. The detailed comparison is presented in Appendix B.

3.2 APPLICATION OF WOODS-SAXON POTENTIAL FOR THE $\gamma \approx 0$ CASE

We consider again the Bohr Hamiltonian in Eq.(2.1.26) to seek the spectrum for the axially symmetric prolate rotor case. At around $\gamma \approx 0$, the last term Eq.(2.1.26) can be written [6] as

$$\sum_{\kappa=1,2,3} \frac{\hat{Q}_\kappa^2}{\sin^2(\gamma - \frac{2\pi\kappa}{3})} \approx \frac{4}{3}(\hat{Q}_1^2 + \hat{Q}_2^2 + \hat{Q}_3^2) + \hat{Q}_3^2(\frac{1}{\sin^2\gamma} - \frac{4}{3}) \tag{3.2.1}$$

Therefore, in this circumstance, Eq. (2.1.26) can be transformed to the forms of

$$H_\beta = -[\frac{1}{\beta^4}\frac{\partial}{\partial\beta}\beta^4\frac{\partial}{\partial\beta} - \frac{1}{4\beta^2}\frac{4}{3}L(L+1)] + u(\beta) \tag{3.2.2}$$

and

$$H_\gamma = -[\frac{1}{\beta^2\sin 3\gamma}\frac{\partial}{\partial\gamma}\sin 3\gamma\frac{\partial}{\partial\gamma} - \frac{1}{4\beta^2}K^2(\frac{1}{\sin^2\gamma} - \frac{4}{3})] + v(\gamma) \tag{3.2.3}$$

If we consider the W-S potential as being $u(\beta)$ and $(3c)^2\gamma^2$ as being $v(\gamma)$, then, bearing in mind that $V(\beta,\gamma) = u(\beta) + \frac{v(\gamma)}{\beta^2}$; $\xi(\beta) = \beta^{-2}\phi(\beta)$ we obviously obtain the familiar expressions [12] below,

$$-\frac{d^2\phi}{d\beta^2} + \left[u(\beta) + \frac{\frac{L(L+1)}{3} + 2 + \lambda}{\beta^2}\right]\phi(\beta) = \varepsilon_{n,\tau}\,\phi(\beta) \tag{3.2.4}$$

and

$$[-\frac{1}{\sin 3\gamma}\frac{\partial}{\partial\gamma}\sin 3\gamma\frac{\partial}{\partial\gamma}+\frac{1}{4}K^2(\frac{1}{\sin^2\gamma}-\frac{4}{3})+v(\gamma)]\eta(\gamma)=\lambda\eta(\gamma) \tag{3.2.5}$$

where

$$\lambda=\varepsilon_\gamma+\frac{K^2}{3};\quad \varepsilon_\gamma=(3C)(n_\gamma+1);\quad n_\gamma=0,1,2...;\quad C=2c$$

$$n_\gamma=0,\quad K=0;\qquad n_\gamma=1,\quad K=\pm2;\qquad n_\gamma=2,\quad K=0,\pm4;\qquad ... \tag{3.2.6}$$

The corresponding eigenvalues of Eq. (3.2.4), in this case, is similar to the case of E(5) with a small difference, in which we need only to replace $\tau(\tau+3)$ term by $\frac{L(L+1)}{3}+2+\lambda$. Thus, the new eigenvalues in this present case, being similar to Eq. (3.1.3), appear as

$$\varepsilon_{n,\tau}^{W-S}=\frac{(\frac{L(L+1)}{3}+2+\lambda)}{\beta_0^2}\left(1+\frac{12a_0^2}{\beta_0^2}\right)-\left\{\frac{\sqrt{1+\left[192(\frac{L(L+1)}{3}+2+\lambda)a_0^4\Big/\beta_0^4\right]}-(2n+1)}{4a_0}\right\}^2-$$
$$\left\{\frac{U_0a_0-8(\frac{L(L+1)}{3}+2+\lambda)a_0^2\Big/\beta_0^3}{\sqrt{1+\left[192(\frac{L(L+1)}{3}+2+\lambda)a_0^4\Big/\beta_0^4\right]}-(2n+1)}\right\}^2-\frac{U_0}{2} \tag{3.2.7}$$

The allowed quantum values are expressed below (note that the condition $I\geq K$ must be fulfilled for the fix K, because K is the projection of I as shown in Fig.2.3 [23].)

$$K = 0, 2, 4, \ldots$$

$$I = \begin{cases} K, K+1, K+2, \ldots & for \quad K \neq 0 \\ 0, 2, 4, \ldots & for \quad K = 0 \end{cases}$$

$$M = -I, -I+1, \ldots, +I$$

$$n_\gamma = 0, 1, 2, \ldots,$$

$$n_\beta = 0, 1, 2, \ldots \tag{3.2.8}$$

With regard to the quantum number, the resultant structure of the lowest ones of these bands is shown schematically in Fig.3.2. As seen below, the ground state band has the levels related to $n_\beta = 0$, $n_\gamma = 0$ with even values of the angular momentum. On the other hand, beta band has the levels of $n_\beta = 1$. Besides, the gama band related to $n_\gamma = 1$ has the odd values of angular momentum as well.

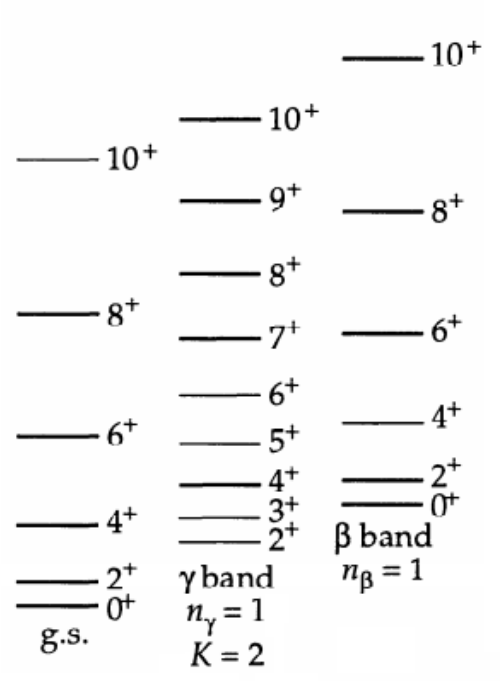

Figure 3. 2: The lowest collective bands

Overall, due to the constraint in Eq.(3.1.4) replacing $(\tau+1)(\tau+2)$ by $(\frac{L(L+1)}{3}+2+\lambda)$, the bandheads and energy spacing of only the ground state and γ bands can be explicitly expressed in the analytical form to produce reliable results just in the $n=0$ case. However, the comparison of our findings with those of experiment for more than 50 medium and heavy mass even-even nuclei in case of X(5) symmetry consideration shows again the success of the present model, as seen in Table(3.2), like the previous E(5) case. The behaviour of the new parameter C, in X(5) case, seems suitable and physically acceptable which can be explained as follow. Approaching to the mid of the shell, both the deformation and surface vibrations intend to increase. Since the harmonic vibration energy is proportional to the parameter C, as approaching to the region of the mid of the shell the value of the parameter C should increase. We can indeed observe these expected behaviours in an explicit manner through Table (3.2), which justifies the reliability of our fixing procedure to predict the potential parameters involving also the new parameter C in the X(5) case. All bands are treated carefully, but on an unequal footing, depending on all four parameters. Results obtained are shown in Table (3.2). The quality measure σ in Eq. (3.1.5), used in the rms fits, remains again below 1 in all considerations, which is significant in such calculations.

Table 3.2 Comparison of theoretical predictions of the Bohr Hamiltonian with the Woods-Saxon potential for axially symmetric prolate deformed nuclei to experimental data [38] of rare earth and actinides with $R_{4/2} > 2.9$ and known 2^+_γ states. The angular momenta of the highest levels of the ground state and quasi-γ bands included in the rms fit are labelled by L_g and L_γ respectively, while N indicates the total number of levels involved in the fit and σ is the quality measure of Eq. (3.1.5). All energies are normalized to the energy of the first excited state, $E(2^+_1)$. For each band, the $R_{4/2} = E(4^+_1)/E(2^+_1)$ ratio (labelled by $4/2$, the normalized bandhead of the quasi-γ band (labelled as $2_\gamma/2$), and the normalized last members of the ground state and quasi-γ_1 bands included in the fit (labelled by $L_g/2$ and $L_\gamma/2$ respectively),are reported. The theoretical predictions are obtained from the Eq. (3.2.7).

Nucleus	$\tilde{\beta}_0$	$\tilde{A}$	C	$\tilde{a}_0$	β_0	V_0	$10^3 a_0$	L_g	L_γ	N	σ	4/2 exp	4/2 th	$L_g/2$ exp	$L_g/2$ th	$2_\gamma/2$ exp	$2_\gamma/2$ th	$L_\gamma/2$ exp	$L_\gamma/2$ th
^{150}Nd	4.1	0.15	7.6	0.62	0.285	207	43	14	4	9	0.24	2.93	3.02	20.6	20.7	8.2	8.6	10.4	9.9
^{152}Sm	4.8	0.20	8.6	0.96	0.306	245	61	16	9	15	0.60	3.01	3.10	27.6	28.0	8.9	10.2	19.5	18.4
^{154}Sm	4.2	0.22	14.0	0.92	0.341	152	75	16	7	13	0.53	3.25	3.26	36.2	36.5	17.6	18.6	26.3	25.0
^{154}Gd	3.4	0.24	6.9	0.82	0.312	119	75	26	7	18	0.35	3.02	3.14	57.3	57.4	8.1	8.8	14.7	14.2
^{156}Gd	2.2	0.24	10.8	0.53	0.338	42	81	26	16	27	0.68	3.24	3.25	74.0	74.1	13.0	14.5	44.9	44.0
^{158}Gd	2.8	0.18	10.6	0.50	0.348	65	63	12	6	10	0.08	3.29	3.28	23.5	23.5	14.9	15.1	20.4	20.3
^{160}Gd	1.8	0.18	9.0	0.32	0.353	26	64	16	8	14	0.10	3.30	3.29	40.0	40.2	13.1	13.1	22.8	22.8
^{162}Gd	1.5	0.18	8.2	0.27				14	4	9	0.05	3.29	3.29	31.4	31.5	12.0	12.0	14.1	14.1
^{156}Dy	3.5	0.24	6.0	0.84	0.293	143	70	28	13	25	0.49	2.93	3.08	57.9	57.9	6.5	7.5	23.8	22.9
^{158}Dy	2.4	0.24	7.7	0.58	0.326	54	78	28	8	20	0.46	3.21	3.21	75.4	74.8	9.6	10.3	19.1	18.2
^{160}Dy	3.0	0.23	9.3	0.69	0.339	78	78	24	23	33	0.88	3.27	3.23	65.1	66.5	11.1	12.5	68.2	69.4
^{162}Dy	1.9	0.19	7.7	0.36	0.343	31	65	18	14	21	0.23	3.29	3.28	47.6	47.9	11.0	11.1	39.4	39.2
^{164}Dy	1.2	0.19	7.1	0.23	0.348	12	66	20	10	18	0.26	3.30	3.28	57.4	58.1	10.4	10.4	25.3	25.3

Table 3.2. (continued)

Nucleus	$\tilde{\beta}_0$	$\tilde{A}$	C	$\tilde{a}_0$	β_0	V_0	$10^3 a_0$	L_g	L_γ	N	σ	4/2 exp	4/2 th	$L_g/2$ exp	$L_g/2$ th	$2_\gamma/2$ exp	$2_\gamma/2$ th	$L_\gamma/2$ exp	$L_\gamma/2$ th
^{166}Dy	1.2	0.15	7.5	0.18				6	5	6	0.02	3.31	3.30	6.9	6.8	11.2	11.2	14.9	14.9
^{160}Er	3.0	0.24	5.6	0.72	0.304	97	73	26	5	16	0.52	3.10	3.11	55.9	55.4	6.8	7.3	10.5	10.0
^{162}Er	1.9	0.24	7.4	0.46	0.322	35	77	20	12	20	0.89	3.23	3.22	43.7	45.4	8.8	10.1	28.5	27.0
^{164}Er	2.1	0.21	6.9	0.44	0.333	40	70	22	16	25	0.61	3.28	3.25	61.8	62.8	9.4	9.8	41.6	43.1
^{166}Er	1.2	0.21	6.9	0.25	0.342	12	72	16	14	20	0.30	3.29	3.26	36.8	37.1	9.8	9.9	35.7	36.6
^{168}Er	1.2	0.16	6.9	0.19	0.338	13	54	18	8	15	0.20	3.31	3.30	50.0	50.6	10.3	10.3	20.4	20.3
^{170}Er	0.7	0.18	8.9	0.13	0.336	4	61	26	19	30	0.85	3.31	3.30	95.8	98.1	11.9	13.0	66.2	65.7
^{162}Yb	2.4	0.25	4.0	0.60	0.263	83	66	24	4	14	0.33	2.92	3.05	39.9	39.1	4.8	5.3	7.1	6.9
^{164}Yb	2.9	0.23	5.6	0.67	0.290	100	67	18	5	12	0.30	3.13	3.14	35.6	35.6	7.0	7.5	10.9	10.3
^{166}Yb	2.4	0.23	7.0	0.55	0.315	58	72	24	13	23	0.82	3.23	3.22	62.3	63.9	9.1	9.6	31.2	30.0
^{168}Yb	3.4	0.22	8.7	0.75	0.322	111	71	34	7	22	0.64	3.27	3.22	120.5	119.7	11.2	11.6	18.5	17.9
^{170}Yb	2.6	0.22	10.1	0.57	0.326	64	72	20	14	22	0.63	3.29	3.26	52.7	54.1	13.6	14.0	39.3	39.9
^{172}Yb	2.2	0.19	13.1	0.42	0.330	44	63	14	5	10	0.11	3.31	3.30	32.0	32.1	18.6	18.8	22.6	22.4
^{174}Yb	2.6	0.20	15.1	0.52	0.325	64	65	18	5	12	0.13	3.31	3.30	50.2	50.4	21.4	21.5	25.2	25.0
^{176}Yb	1.8	0.20	10.7	0.36	0.305	35	61	18	5	12	0.29	3.31	3.29	48.4	49.0	15.4	15.3	19.0	18.9
^{178}Yb	1.3	0.17	9.9	0.22				6	2	3	0.01	3.31	3.30	6.9	6.9	14.5	14.5	14.5	14.5
^{166}Hf	2.2	0.25	4.1	0.55	0.250	77	63	22	3	12	0.24	2.97	3.08	36.9	36.5	5.1	5.5	6.3	6.2
^{168}Hf	2.5	0.24	5.7	0.60	0.275	83	66	22	4	13	0.28	3.11	3.16	46.5	46.9	7.1	7.7	9.8	9.4
^{170}Hf	3.9	0.22	7.9	0.86	0.301	168	66	34	4	19	0.48	3.19	3.16	105.7	105.3	9.5	10.1	12.2	11.7
^{172}Hf	3.4	0.23	9.0	0.78	0.276	152	63	38	6	23	0.69	3.25	3.21	132.8	133.5	11.3	11.9	17.0	16.3

Table 3.2.(continued)

Nucleus	$\tilde{\beta}_0$	$\tilde{A}$	C	$\tilde{a}_0$	β_0	V_0	$10^3 a_0$	L_g	L_γ	N	σ	4/2 exp	4/2 th	$L_g/2$ exp	$L_g/2$ th	$2_\gamma/2$ exp	$2_\gamma/2$ th	$L_\gamma/2$ exp	$L_\gamma/2$ th
^{174}Hf	3.1	0.23	10.2	0.71	0.286	117	66	22	4	13	0.43	3.27	3.24	58.2	58.9	13.5	13.7	15.9	15.5
^{176}Hf	2.9	0.22	11.4	0.64	0.295	96	65	18	6	13	0.34	3.28	3.27	45.4	45.7	15.2	15.7	21.1	20.6
^{178}Hf	2.2	0.22	9.2	0.48	0.280	62	62	18	6	13	0.41	3.29	3.26	44.2	45.0	12.6	12.9	18.1	17.8
^{180}Hf	1.0	0.16	8.7	0.16	0.274	13	44	12	5	9	0.05	3.31	3.30	24.3	24.4	12.9	12.9	16.7	16.6
^{176}W	2.4	0.24	7.6	0.58				22	5	14	0.31	3.22	3.21	51.8	51.8	9.6	10.2	14.0	13.2
^{178}W	2.4	0.23	7.6	0.55				14	2	7	0.14	3.24	3.23	27.0	27.2	10.5	10.4	10.5	10.4
^{180}W	2.7	0.24	8.7	0.65	0.254	113	61	24	7	17	0.67	3.26	3.22	60.0	60.4	10.8	11.6	18.7	17.6
^{182}W	1.4	0.20	8.6	0.28	0.251	31	50	18	6	13	0.26	3.29	3.28	47.4	48.0	12.2	12.4	17.7	17.6
^{184}W	0.9	0.18	5.4	0.16	0.236	15	43	10	6	9	0.06	3.27	3.28	16.7	16.8	8.1	8.0	13.3	13.4
^{186}W	1.0	0.19	4.1	0.19	0.226	20	43	14	6	11	0.09	3.23	3.25	29.1	29.2	6.0	6.1	11.4	11.4
^{176}Os	4.0	0.23	6.0	0.92				24	5	15	0.37	2.93	3.04	45.5	45.5	6.4	7.3	10.4	9.6
^{178}Os	3.8	0.23	6.0	0.87				16	5	11	0.40	3.02	3.06	26.1	26.0	6.6	7.4	10.8	9.9
^{180}Os	2.5	0.25	5.9	0.63	0.226	122	57	14	7	12	0.59	3.09	3.14	21.8	22.0	6.6	7.7	14.2	13.0
^{182}Os	3.7	0.24	6.7	0.89	0.234	250	56	26	7	18	0.84	3.15	3.10	54.0	53.3	7.0	8.3	14.6	13.4
^{184}Os	2.2	0.24	6.2	0.53	0.213	107	51	22	6	15	1.05	3.20	3.19	47.9	49.4	7.9	8.4	13.5	12.8
^{186}Os	1.7	0.22	4.2	0.37	0.200	72	44	14	13	18	0.20	3.17	3.19	25.9	26.1	5.6	6.1	26.5	26.8
^{188}Os	1.4	0.23	3.0	0.32	0.186	57	43	12	7	11	0.18	3.08	3.14	18.4	18.7	4.1	4.4	10.9	10.6
^{190}Os	1.4	0.24	2.2	0.34	0.178	62	43	10	6	9	0.20	2.93	3.06	12.6	12.7	3.0	3.3	7.9	7.6
^{228}Ra	3.1	0.24	10.1	0.74	0.217	204	52	22	3	12	0.18	3.21	3.23	53.6	54.0	13.3	13.3	14.1	14.0
^{228}Th	3.5	0.24	13.1	0.84	0.230	231	55	18	5	12	0.15	3.24	3.25	41.7	41.6	16.8	17.1	20.3	20.0

Table 3.2. (continued)

Nucleus	$\tilde{\beta}_0$	$\tilde{A}$	C	$\tilde{a}_0$	β_0	V_0	$10^3 a_0$	L_g	L_γ	N	σ	4/2 exp	4/2 th	$L_g/2$ exp	$L_g/2$ th	$2_\gamma/2$ exp	$2_\gamma/2$ th	$L_\gamma/2$ exp	$L_\gamma/2$ th
^{230}Th	2.8	0.22	10.6	0.62	0.244	132	54	18	4	11	0.12	3.27	3.26	45.1	45.3	14.7	14.7	16.6	16.6
^{232}Th	2.4	0.23	12.1	0.55	0.261	85	60	30	12	25	0.54	3.28	3.27	104.6	105.9	15.9	16.6	36.5	35.6
^{232}U	3.0	0.22	13.3	0.66	0.264	129	58	20	4	12	0.20	3.29	3.28	55.9	56.3	18.2	18.4	20.4	20.3
^{234}U	2.7	0.23	15.9	0.62	0.272	99	63	28	7	19	0.36	3.30	3.29	98.8	99.6	21.3	21.8	29.0	28.5
^{236}U	3.3	0.22	15.5	0.73	0.282	137	62	26	5	16	0.63	3.30	3.29	89.3	90.6	21.2	21.4	24.9	24.7
^{238}U	2.9	0.23	18.3	0.67	0.286	103	66	30	27	40	0.85	3.30	3.29	112.1	114.9	23.6	25.0	112.7	113.5
^{238}Pu	1.7	0.21	16.5	0.36	0.286	35	60	26	4	15	0.34	3.31	3.30	96.8	97.6	23.3	23.4	25.5	25.5
^{240}Pu	2.2	0.22	19.0	0.48	0.289	58	64	26	4	15	0.21	3.31	3.30	95.5	96.0	26.6	26.6	28.8	28.6
^{242}Pu	2.3	0.22	17.7	0.51	0.292	62	64	26	2	13	0.51	3.31	3.30	93.7	94.8	24.7	24.8	24.7	24.8
^{248}Cm	2.7	0.22	17.2	0.59	0.297	83	65	28	2	14	0.87	3.31	3.30	10.5	10.7	24.2	24.0	24.2	24.0
^{250}Cf	2.2	0.17	16.6	0.37	0.299	54	51	8	4	6	0.02	3.32	3.31	11.7	11.7	24.2	24.1	26.3	26.3

The behaviour of W-S potentials obtained for the $_{70}Yb$ isotopes are illustrated by Fig.3.3, in which $^{162}Yb_{92}$ is the deepest one while $^{174}Yb_{104}$ is in the middle of the shell where shallow potentials occur. The 4_g value is indeed increasing as we move from ^{162}Yb to ^{176}Yb. Apart from this, the same observation as in Fig.3.1 in connection with the potential parameters V_0, a_0 and β_0 appears in Fig.3.3, too, for the deformed nuclei underlined and the potentials shift slightly as we move to ^{176}Yb. The C parameter, which is related to the stiffness of the $\gamma-$ potential, increases as one moves to $^{176}Yb_{104}$ as shown in Table 3.2. As a result, one gradually obtains less steep $\beta-$potentials with a minimum farther away from the origin, while the $\gamma-$potentials get stiffer at the same time.

Moreover, from Table 3.2, it is clear that the extra parameter (V_0, a_0, β_0, C) when compared to the earlier calculations extends the region of applicability of the model in most nuclei to higher angular momenta, largely improving the quality of the fits. In addition, as expressed in the previous section, the physical investigation of the Pekeris approximation for the $\gamma \approx 0$ case is also considered in Appendix B.

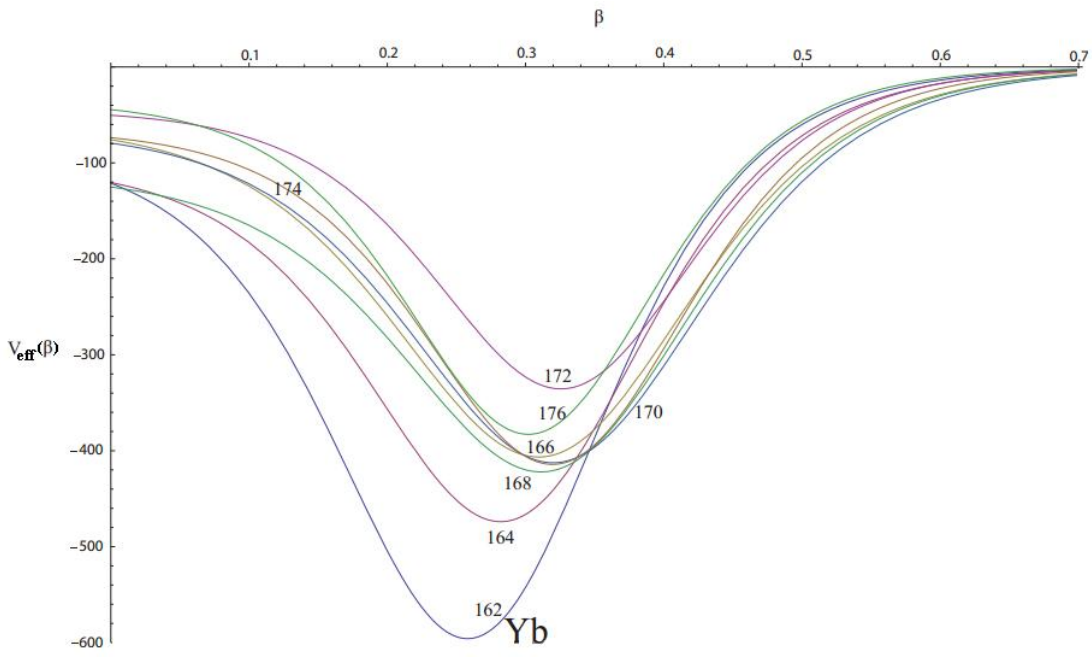

Figure 3. 3: Behaviour of the Woods-Saxon potentials used for the $_{70}Yb$ isotopes for an arbitrary $L(=10)$ value.

CHAPTER 4

CONCLUSION

In this work, which has been supported by the Scientific and Technical Research Council of Turkey (TÜBİTAK) with the project number of ARDEB/1002-113F218, we have produced reliable analytical solutions of the Bohr Hamiltonian with the Woods-Saxon potential in five dimensions to predict the structure of deformed even-even nuclei, which was missing in the related literature.

We stress however that, due to the mathematical constraint arisen naturally in the formalism, one can compute only the lowest bands in the case of $n = 0$ within the frame of the new model to analyse medium/heavy mass even-even nuclei. In the other words, the bandheads and energy spacings belonging solely to the ground state and γ bands can be safely predicted through the flexible framework of the present calculation technique. However, the mathematical constraints expressed during the thesis force us to choose the suitable parameters. For the most cases of $n = 1$ which corresponds to beta-band, the some related parameters have violated the constraints and led us to the conclusion that such an investigation cannot be proceed by the potential used through the calculations, unlike the other band analysis.

We believe that the other possible reason concerning the failure of the W-S potential in describing beta bands is due to the lack of a hard core [41]. The earlier potentials used in the literature to describe beta bands, like Davidson, Kratzer, Morse, all have a hard core, not allowing the nucleus to reach $\beta \simeq 0$ region. Within this context, through the present work, we have answered an interesting question that arises naturally considering the success of the mentioned potentials: Are these successes due to the form of the Bohr Hamiltonian alone involving such potentials with a hard core or if there are potentials which, when plugged into the Bohr Hamiltonian, will not be able to provide satisfactory results for nuclear data?

Along this line, we have observed that the Woods-Saxon potential can describe only the ground state and γ bands equally well as other potentials (Davidson, Kratzer, Morse), but it fails to describe the β band, apparently because of its lack of a hard core as shown in Figure 4.1. Bohr Equation implies the parameter of the Woods-Saxon potential to obtain values producing a very large dip near its surface that is illustrated by Figure 2.7., so that its overall shape around the minimum largely resembles the shape around the minimum of the Davidson, or the Kratzer, or the Morse potential. The lack of a hard core does not decisively affect the description of the ground state and γ bands, but destroys the ability of the potential to describe β band. It is therefore concluded that potentials used in the Bohr Hamiltonian can provide satisfactory results for nuclear spectra if they possess two features, a hard core and a deep oscillator-like minimum.

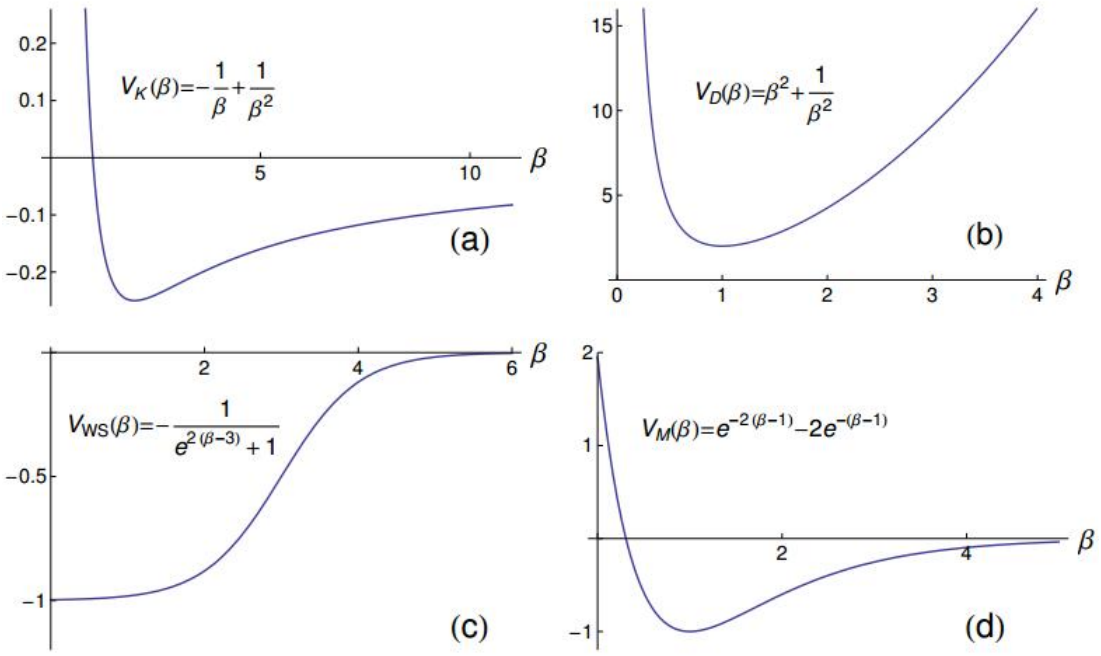

Figure 4.1: The Kratzer [42] (a), Davidson [43] (b), Woods–Saxon [13] (c) and Morse [44] (d) potentials, for special values of their free parameters, used for simplicity. All quantities shown are dimensionless.

On the other hand, unlike some incorrect discussions in the literature [16-19], one concludes, considering the whole work presented in this thesis, that the standard Woods-Saxon potential plugged into the Bohr Hamiltonian cannot describe nuclei, unless it is distorted into a potential with a large dip near its surface by means of additional parameter, W.

Another important issue, before the applications like the ones performed in this thesis work is to make sure from the validity of the Pekeris approximation used through such investigations. Our exhaustive analysis however, which has been well discussed for the reader in Appendix B, describes in an explicit manner that how one finds a physically meaningful way for the certain definition of the domains where the approximation used works successfully or fails. This is indeed a significant milestone in such calculations.

Apart from this, the potential parameters used for the present calculations for both ground state and γ bands are found as fairly suitable and physically acceptable, which means that the fixing procedure used here for this purpose is reliable. Approaching the mid-shell region where the collective behaviour reaches maximum, we see that the parameters a_0, β_0, C increase while the parameter V_0 decreases, as expected, which are well expressed in detail through the related sections. Besides, we have clearly shown here that the model results are in well agreement with experiment, particularly for higher angular momentum values.

For the completeness, some additional detailed calculations on $B(E2)$ transitions are certainly required to test also the reliability of the wavefunction introduced by the new potential definition in this thesis work. Such transitions refer to the electric quadrupole transitions and allow the determination of the intrinsic quadrupole moments related to the charge distribution inside nuclei, and thus the deformation itself. The related work is in progress. The required initial calculation framework is presented in Appendix C.

REFERENCES

[1] Rainwater, J., (1950), Nuclear Energy Level Argument for a Spheroidal Nuclear Model, *Physical Review*, **79**, 432-434.

[2] Bohr, A., (1952), The Coupling of Nuclear Surface Oscillations to the Motion of Individual Nucleons, *Det Kongelige Danske Videnskabernes Selskab Matematisk-fysiske Meddelelser*, **26, No.14**, 1-40.

[3] Bohr, A. and Mottelson, B. R., (1955), Moments of Inertia of Rotating Nuclei, *Det Kongelige Danske Videnskabernes Selskab Matematisk-fysiske Meddelelser*, **30, No.1**, 1-24.

[4] Bohr, A. and Mottelson, B. R., 1975, Nuclear Structure Vol.II: Nuclear Deformations , New York, Benjamin.

[5] Iachello, F., (2000), Dynamic Symmetries at the Critical Point, *Physical Review Letters*, **85**, 3580-3583.

[6] Iachello, F., (2001), Analytic Description of Critical Point Nuclei in a Spherical-Axially Deformed Shape Phase Transition, *Physical Review Letters*, **87**, 052502.

[7] Caprio, M., A., (2002), Finite Well Solution for the E(5) Hamiltonian, *Physical Review C*, **65**, 031304.

[8] Fortunato, L. and Vitturi, A., (2003), Analytically Solvable Potentials for $\gamma-$unstable Nuclei, *Journal of Physics G: Nuclear and Particle Physics*, **29**, 1341-1349.

[9] Levai, G. and Arias, J. M., (2004), The Sextic Oscillator as a $\gamma-$independent Potential, *Physical Review C*, **69**, 014304.

[10] Bonatsos, D., Lenis, D., Minkov, N., Petrellis, D., Raychev, P. R., Terziev, P. A., (2004) Ground State Bands of the E(5) and X(5) Critical Symmetries Obtained from Davidson Potentials Through a Variational Prodecure, *Physics Letters B*, **584**, 40-47.

[11] Bonatsos, D., Lenis, D., Minkov, N., Raychev, P. R., Terziev, P. A., (2004), Sequence of Potentials Lying Between the U(5) and X(5) Symmetries, *Physical Review C*, **69**, 014302.

[12] Boztosun, I., Bonatsos, D. and Inci, I., (2008), Analytical Solutions of the Bohr Hamiltonian with the Morse Potential, *Physical Review C*, **77**, 044302.

[13] Woods, R.D., Saxon, D.S., (1954), Diffuse Surface Optical Model for Nucleon-Nuclei Scattering, *Physical Review*, **95**, 577.

[14] Pekeris, C.L., The Rotation-Vibration Coupling in Diatomic Molecules**,** *Physical Review*, (1934), **45**, 98.

[15] Flügge, S., 1994, Practical Quantum Mechanics, Vol. 1, Berlin, Springer.

[16] Saha, A., Das, U. and Talukdar, (2011), On Eigenvalue Problems in Quantum Mechanics, B., *Physica Scripta*, **83**, 65003.

[17] Feizi, H., Rajabi, A.A., Shoajei, M.R., (2011), Supersymmetric Solution of the Schrödinger Equation for Woods–Saxon Potential by Using the Pekeris Approximation, *Acta Physica Polonica B***, 42**, 2143.

[18] Berkdemir, C., Berkdemir, A. and Sever, R., (2005), Polynomial Solutions of the Schrödinger Equation for the Generalized Woods-Saxon Potential , *Physical Review C*, **72**, 27001; (2006), *Physical Review C*, **74**, 39902(E).

[19] Ikhdair, S. M., Falaye, B. J. and Hamzavi, M., (2013), Approximate Eigensolutions of the Deformed Woods-Saxon Potential via AIM, *Chinese Physics Letters*, **30, No.2**, 020305.

[20] Gönül, B. and Köksal, K., (2007), Solutions for a Generalized Woods–Saxon Potential, *Physica Scripta*, **76**, 565.

[21] Badalov, V.H., Ahmadov, H.I. and Ahmadov, A.I (2009), Analytıcal Solutıons of the Schrödınger Equatıon wıth the Woods–Saxon Potentıal for Arbıtrary l-state , *International Journal of Modern Physics E*, **18, No:03**, 631; Badalov, V.H., Ahmadov, H.I., (2011), Analytical Solutions of the D-dimensional Schrodinger Equation with the Woods-Saxon Potential for Arbitrary l-state, math-phys/1111.4734

[22] Heyde, K., 1999, Basic Ideas and Concepts in Nuclear Physics-An Introductory Approach, Bristol, Institute of Physics Publishing.

[23] Greiner, W. and Maruhn, J. A., 1996, Nuclear Models, New York, Springer-Verlag.

[24] Podolsky, B., (1928), Quantum-Mechanically Correct Form of Hamiltonian Function for Conservative Systems, *Physical Review*, **32**, 812.

[25] Sitenko, A. G. and Tartakovski V. K., 1975, Lectures on the Theory of the Nucleus, Pergamon, Oxford.

[26] Casten, R. F. and McCutchan, E. A., (2007), Quantum Phase Transitions and Structural Evolition in Nuclei, *Journal of Physics G: Nuclear and Particle Physics*, **34**, R285-R320.

[27] Koura, H. and Yamada, M., (2000), Single-particle Potentials for Spherical Nuclei, *Nuclear Physics A*, **671**, 96.

[28] Berkdemir, C., Berkdemir, A. and Sever, R., (2008), Shape-invariance Approach and Hamiltonian Hierarchy Method on the Woods–Saxon Potential for $\ell \neq 0$ states, *Journal of Mathematical Chemistry,* **43**, 944.

[29] Ikhdair, S. M. and Sever, R., (2007), Exact Polynomial Solution of PT-/Non-PT-Symmetric and Non-Hermitian Modified Woods–Saxon Potential by the Nikiforov–Uvarov Method, *International Journal of Theoretical Physics,* **46**, 1643.

[30] Berkdemir, C., Berkdemir, A. and Sever, R., (2006), Eigenvalues and Eigenfunctions of Woods–Saxon Potential in Pt-symmetric Quantum Mechanics, *Modern Physics Letters A*, **21, No: 27**, 2087.

[31] Fakhri, H. and Sadeghi, J., (2004), Supersymmetry Approaches to the Bound States of the Generalized Woods-Saxon Potential, *Modern Physics Letters A*, **19**, 615.

[32] Costa, L.S., Prudente, F.V., Acioli, P.H., Neto, J.J.S. and Vianna, J.D.M., (1999), A Study of Confined Quantum Systems Using the Woods-Saxon Potential, *Journal of Physics B: Atomic, Molecular and Optical Physics*, **32**, 2461.

[33] Eğrifes, H., Demirhan, D. and Büyükkılıç, F., (1999), Polynomial Solutions of the Schrödinger Equation for the "Deformed" Hyperbolic Potentials by Nikiforov–Uvarov Method, *Physica Scripta*, **59**, 90.

[34] Gönül, B., Özer, O., Koçak, M., Tutcu, D. and Cançelik, Y., (2001), Supersymmetry and the Relationship Between a Class of Singular Potentials in Arbitrary Dimensions, *Journal of Physics A: Mathematical and General*, **34**, 8271; Gönül, B. and Koçak, M., (2006), Explicit Solutions for ***N***-dimensional Schrödinger Equations with Position-dependent Mass, *Journal of Mathematical Physics*, **47**, 102101.

[35] Bes, D. R., (1959), The γ – dependent Part of the Wave Functions Representing γ – unstable Surface Vibrations, *Nuclear Physics*, **10**, 373-385.

[36] Rakavy, G., (1957), The Classification of States of Surface Vibrations, *Nuclear Physics*, **4**, 289.

[37] Raman, S., Nestor, C. W. Jr. and Tikkanen, P., (2001), Transition Probability from the Ground to the First-excited 2^+ state of Even–even Nuclides, *Atomic Data and Nuclear Data Tables*, **78**, 1.

[38] Brookhaven National Laboratory, National Nuclear Data Center, Evaluated Nuclear Structure Data File, http://www.nndc.bnl.gov/ensdf/

[39] İnci, İ., 2010, Analysis of Quantum Phase Transitions in Medium-Heavy and Heavy Mass Nuclei , Ph.D. Thesis, University of Erciyes.

[40] Bonatsos, D., McCutchan E. A., Minkov, N., Casten, R. F., Yotov, P., Lenis, D., Petrellis, D., Yiğitoğlu, İ.,(2007), Exactly Separable Version of the Bohr Hamiltonian with the Davidson Potential, *Physical Review C*, **76**, 064312.

[41] Bonatsos, D., Lenis, D., Pietralla, N., Terziev, P. A., (2006), γ-soft analog of the confined β-soft rotor model, *Physical Review C*, **74**, 044306.

[42] Kratzer, A., (1920), The Infra-red Rotational Spectra of Hydrogen Halides, *Zeitschrift für Physik*, **3**, 289.

[43] Davidson, P. M., (1932), Eigenfunctions for Calculating Electronic Vibrational Insensities, *Proceedings of the Royal Society of London Series A*, **135**, 459.

[44] Morse, P. M., (1929), Diatomic Molecules According to the Wave Mechanics. II. Vibrational Levels, *Physical Review*, **34**, 57.

[45] Çapak, M., Petrellis, D., Gönül, B. and Bonatsos, D., (2015), Analytical Solutions for the Bohr Hamiltonian with the Woods-Saxon Potential, *Journal of Physics G: Nuclear and Particle Physics*, **42**, 095102.

APPENDIX A: PHYSICAL MEANING OF β_0 IN THE EFFECTIVE POTENTIAL

It is instructive to study the physics behind the parameter β_0 appeared in Eq.(3.1.3) for the case of Bohr Hamiltonian consideration, which corresponds in fact to the average radius of the nucleus of interest for the three dimensional consideration as in Eqs. (2.3.12) and (2.3.16) while the strength of the effective potential in (2.3.12) within the five dimensional framework of the Bohr Hamiltonian reduces to

$$U_{eff}\left(\beta_0\right) = -\left(U_0 - \delta C_1\right)/2 + \left(\delta C_2/4\right) \tag{A.1}$$

for $\beta = \beta_0$ case which will be re-considered below. To understand, first, the connection between the actual minimum $\left(\beta_{\min}\right)$ of the corresponding effective potential used in the frame of the Bohr Hamiltonian and β_0 we first equate the derivative of the potential to zero such that

$$\frac{\partial}{\partial\beta}\left[U_{eff}(r)\right] = \frac{\partial}{\partial\beta}\left\{-\frac{\left(U_0 - \delta C_1\right)}{\left[e^{(\beta-\beta_0)/a_0}+1\right]} + \frac{\delta C_2}{\left[e^{(\beta-\beta_0)/a_0}+1\right]^2}\right\} = 0 \tag{A.2}$$

which, after some simple algebra, leads to

$$\beta_{\min} = \beta_0 + a_0 \ln\left(\frac{2\delta C_2}{U_0 - \delta C_1} - 1\right) \tag{A.3}$$

that clarifies explicitly the relation between $\beta_{\min}$ and β_0 points. It is obvious that if $U_0 = \delta\left(C_1 + C_2\right)$, which is the lower limit for physically acceptable U_0 as discussed through Eqs. (2.3.7)-(2.3.14), then $\beta_{\min} = \beta_0$ case occurs in this threshold which causes the Woods-Saxon potential in (A.2) to die away. This disappearance occurs even in the low dimensional cases $\left(V_0 \to 0\right)$, that can be visualized by the consideration of Eqs. (2.3.1), (2.3.4), (2.3.12) and (2.3.14) within the unique frame in case $U_0 = \delta\left(C_1 + C_2\right)$. Hence, the real minimum of the potential in any case should be smaller than its upper threshold value, β_0, as presented by (A.3). For this reason, leading to physically acceptable $\beta_{\min}$ values, the $\frac{1}{2} < \frac{\delta C_2}{U_0 - \delta C_1} < 1$ condition in (A.3) must be certainly satisfied in order to have physically reasonable interval for U_0 values

$$\frac{(\tau+1)(\tau+2)}{\beta_0^2}\left(\frac{8a_0}{\beta_0}\right) < U_0 < \frac{(\tau+1)(\tau+2)}{\beta_0^2}\left(\frac{8a_0}{\beta_0} + \frac{48a_0^2}{\beta_0^2}\right) \tag{A.4}$$

which will be useful in defining the potential parameters in the present calculations.

It would be convenient at this stage to understand also the interplay between U_0 and the actual minimum of the corresponding effective potential. The substitution of (A.3) in $U_{eff}\left(\beta\right)$ appeared in (A.2), with $\beta \to \beta_{\min}$, yields the minimum of the effective potential in the explicit form

$$U_{eff}\left(\beta_{\min}\right) = -\frac{\left(U_0 - \delta C_1\right)^2}{4\left(\delta C_2\right)} = -\frac{\left[U_0 - \frac{(\tau+1)(\tau+2)}{\beta_0^2}\left(\frac{8a_0}{\beta_0} - \frac{48a_0^2}{\beta_0^2}\right)\right]^2}{4\left[\frac{(\tau+1)(\tau+2)}{\beta_0^2}\left(\frac{48a_0^2}{\beta_0^2}\right)\right]} \tag{A.5}$$

that puts another constraint for the physically meaningful $U_{eff}(\min)$ values with the consideration of the possible interval given by (A.4). Furthermore, bearing in mind Eqs. (A.1) and (A.5) together with the lower limit $U_0 = \delta(C_1 + C_2)$, the equality $U_{eff}(\beta_0) = U_{eff}(\beta_{\min}) = -\delta C_2/4$ at $\beta_{\min} = \beta_0$ case justifies the whole discussion above.

APPENDIX B: VALIDITY OF THE PEKERIS APPROXIMATION

In order to examine the reliability of the Pekeris approximation used in the present thesis work, we compare both the original exact potential (dashed line) obtained from Eq. (2.3.7) and the approximate potential (solid line), via the Pekeris approximation, obtained from Eq. (2.3.12) in the same graphs for the six different values of angular momenta in the case of ^{232}Th, as well the relevant energy levels (straight line), replacing $l(l+1)$ by $\frac{L(L+1)}{3} + \lambda + 2$ in which $\lambda = 3C$.

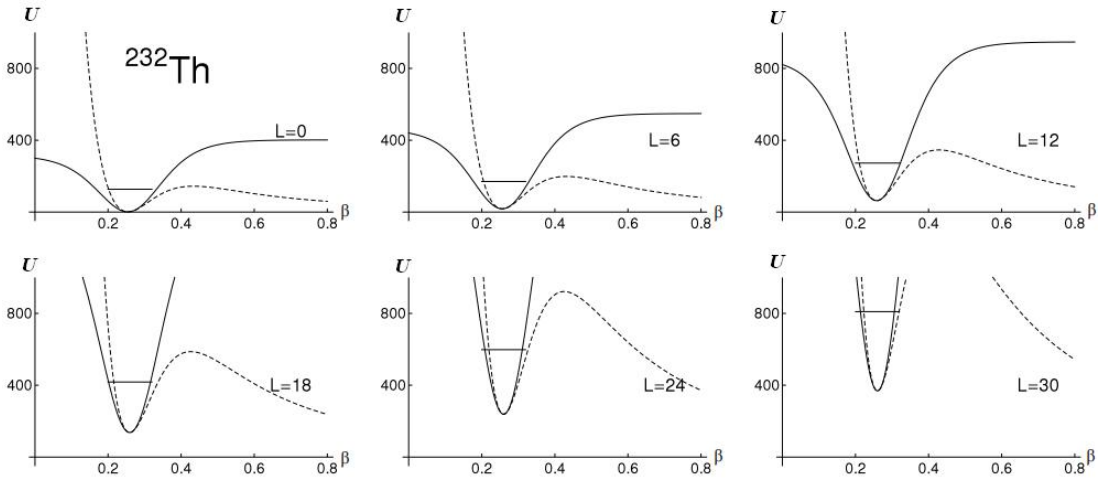

Figure B. 1: For ^{232}Th, exact (dashed lines) and approximate (solid lines) potentials in case of six different values of angular momentum, $L = 0, 6, 12, 18, 24, 30$, as well the relevant energy levels (straight lines).

For all of the values of angular momentum, the exact and the approximate potentials coincide in minima, and the wells around the minima have similar forms.

As more importantly, the relevant energy levels are inside the exact potential wells as expected. Though the approximation works well for some nuclei, for example ^{232}Th, in the case of some nuclei it breaks down, unfortunately. For clarifying this point, it would be appropriate to compare graphs of ^{170}Yb and ^{176}Yb.

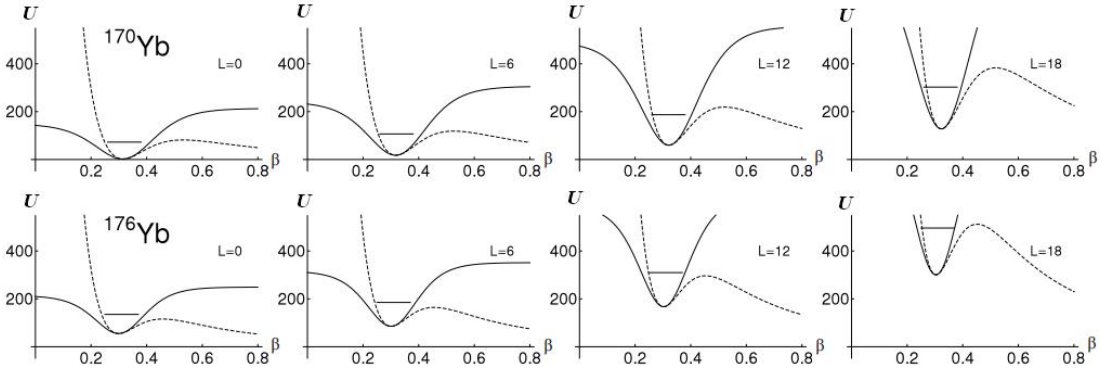

Figure B. 2: Comparing the exact and approximate potentials for ^{170}Yb and ^{176}Yb in the case of four different values of angular momentum, $L = 0, 6, 12, 18$.

While the Pekeris approximation meets the expectation for ^{170}Yb described above, it breaks down for ^{176}Yb since, especially for low values of L, the relevant energy levels lie higher than corresponding barriers of the exact potential. After consideration of all of the nuclei in this context, we see that the approximation breaks down for "well size" $\tilde{\beta}_0 \leq 1.8$ and/or diffuseness $\tilde{a}_0 \leq 0.43$. This result is reasonable, because for low values of β_0, the rotational term in which the Pekeris approximation has been used becomes over effective, thus the approximation deteriorates the exact potential. Therefore in the case of the nuclei that have parameter values of $\tilde{\beta}_0 \geq 1.9$ and/or $\tilde{a}_0 \geq 0.44$, the approximate potentials are similar to the exact potentials.

Consequently, considering our detailed exhaustive analysis [45], one concludes that the Pekeris approximation breaks down for the $\gamma-$unstable nuclei in Table 3.1, as well the nuclei $^{160-162}Gd$, $^{162-164-166}Dy$, $^{166-168-170}Er$, $^{172-176-178}Yb$, ^{180}Hf, $^{182-184-186}W$, $^{186-188-190}Os$, ^{238}Pu, ^{250}Cf in the list of $\gamma \approx 0$ (Table 3.2). Nevertheless, we have overall good fits for all these nuclei when compared to the experimental

data which are astonishingly obtained using the approximate potential underlined, but this potentials are not similar to the exact potentials any more, unlike the others for which the Pekeris approximation works well as in ^{232}Th, preventing us to reach any conclusions regarding the exact potentials in which it breaks down.

APPENDIX C: ELECTRIC QUADRUPOLE TRANSITION, B(E2)

Electric quadrupole transitions between collective levels, B(E2), are another important manifestation of the Collective Model discussed throughout the present thesis work. The related transitions occur due to the change of the nuclear charge distribution depending on the shape-deformation. To perform the necessary calculations, one needs to consider the required wavefunctions in an explicit manner.

C1. B(E2) TRANSITIONS IN THE CASE OF $\gamma-$ UNSTABLE

For this case, the wave function is considered as

$$\Psi(\beta,\gamma,\theta_i) = f(\beta)\Phi^{I,\tau}_{M,K}(\gamma,\theta_i) \tag{C.1}$$

where $f(\beta) = \beta^{-2}\phi(\beta)$. In addition, $\Phi^{I,\tau}_{M,K}$ is expressed by Wigner functions, $D^{I}_{M,K}(\theta_I)$, and given as below[39]

$$\Phi(\gamma,\theta_i) = \frac{1}{\sqrt{A_\tau}}\left(\frac{\alpha_2}{\beta}\right)^{\tau} \quad ; \quad A_\tau = 16\pi^2\frac{\tau!}{(2\tau+3)!!}$$

$$\alpha_\mu = \beta\left[\cos\gamma D^{(2)}_{\mu,0}(\theta_i) + \frac{\sin\gamma}{\sqrt{2}}\left(D^{(2)}_{\mu,2}(\theta_i) + D^{(2)}_{\mu,-2}(\theta_i)\right)\right] \tag{C.2}$$

where I is the quantum number related to angular momentum while M and K are the projections of I on the laboratory-fixed and body-fixed frames, respectively. The normalization condition and the volume element are given as

$$1=\int_{\beta=0}^{\infty}\int_{\gamma=0}^{\pi/3}\int_{\theta_1=0}^{2\pi}\int_{\theta_2=0}^{\pi}\int_{\theta_3=0}^{2\pi}\Psi^{*}(\beta,\gamma,\theta_1,\theta_2,\theta_3)\Psi(\beta,\gamma,\theta_1,\theta_2,\theta_3)dv$$

$$dv=\beta^4 d\beta\left|\sin 3\gamma\right| d\gamma d\theta_1 \sin\theta_2 d\theta_2 d\theta_3 \tag{C.3}$$

Considering Eq.(2.3.3) and the discussion in Chapter 3, we see that $\phi(\beta)$ has the form below

$$\phi_n(\beta)\propto\left[\frac{1}{e^{\frac{(\beta-\beta_0)}{a_0}}+1}\right]^{b/2}\left[1-\frac{1}{e^{\frac{(\beta-\beta_0)}{a_0}}+1}\right]^{c/2}P_n^{(b,c)} \tag{C.4}$$

with

$$b=\frac{1}{2}\left[\sqrt{1+W(4a_0^2)}-(2n+1)+\frac{V(4a_0^2)}{\sqrt{1+W(4a_0^2)}-(2n+1)}\right]$$

$$c=\frac{1}{2}\left[\sqrt{1+W(4a_0^2)}-(2n+1)-\frac{V(4a_0^2)}{\sqrt{1+W(4a_0^2)}-(2n+1)}\right] \tag{C.5}$$

where $W=\dfrac{(\tau+1)(\tau+2)}{(\beta_0^2)}\left(\dfrac{48(a_0^2)}{(\beta_0^2)}\right)$ and $P_n^{(b,c)}$ are the Jacobi polynomials. In this case, B(E2) values can be expressed as below with respect to the quadrupole operators[5],

$$T_{\mu}^{(E2)} = t\alpha_{\mu} = t\beta\left[\cos\gamma D_{\mu,0}^{(2)}(\theta_i) + \frac{\sin\gamma}{\sqrt{2}}\left(D_{\mu,2}^{(2)}(\theta_i) + D_{\mu,-2}^{(2)}(\theta_i)\right)\right] \tag{C.6}$$

where t is a scalar factor. Then,

$$B(E2; n_i, L_i \to n_f, L_f) = \frac{1}{2L_i+1}\left|\left\langle n_f, L_f \left\| T^{(E2)} \right\| n_i, L_i \right\rangle\right|^2$$

$$= \frac{2L_f+1}{2L_i+1} B(E2; n_f, L_f \to n_i, L_i) \tag{C.7}$$

Finally, B(E2) rates seems as Ref.[39],

$$R_{n,L}^{B(E2)} = \frac{B\left[E2; (L+2)_{n',\tau+1} \to L_{n,\tau}\right]}{B\left(E2; 2_0 \to 0_0\right)} \tag{C.8}$$

in which

$$B(E2; (L+2)_{n',\tau+1} \to L_{n,\tau}) = \frac{(\tau+1)}{(2\tau+5)} t^2 I_{n',\tau+1,n,\tau}^2 \tag{C.9}$$

and

$$B(E2; L_{n,\tau} \to (L+2)_{n',\tau+1}) = \frac{(\tau+1)(4\tau+1)}{(2\tau+5)(4\tau+1)} t^2 I_{n',\tau+1,n,\tau}^2 \tag{C.10}$$

where $I_{n',\tau+1,n,\tau} = \int_0^{\infty} \beta^5 f_{n',\tau+1}(\beta) f_{n,\tau}(\beta) d\beta$ and $L = 2\tau$.

C2. B(E2) TRANSITIONS IN THE CASE OF $\gamma \approx 0$

For this case, the wavefunction is given as below [40]

$$\Psi(\beta,\gamma,\theta_i) = f_L(\beta)\eta_K(\gamma)D^L_{M,K}(\theta_i) \tag{C.11}$$

$$\Psi(\beta,\gamma,\theta_i) = f_L(\beta)\eta_K(\gamma)\sqrt{\frac{2L+1}{16\pi^2(1+\delta_{K,0})}}\left[D^L_{M,K}(\theta_i) + (-1)^L D^L_{M,-K}(\theta_i)\right] \tag{C.12}$$

ın which

$$\eta_{n,\gamma,|K|}(\gamma) = C_{n,\gamma,|K|}\gamma^{|K/2|}e^{-(3c)\gamma^2/2}L^{|K/2|}_{\tilde{n}}(3c\gamma^2) \tag{C.13}$$

where $L^{|K/2|}_{\tilde{n}}(3c\gamma^2)$ is the well known Laguerre polynomials. For this case, the wave function description in connection with β is similar to the previous case, but with a small difference [20] , such as

$$f(\beta) = \beta^{-2}\phi(\beta) \tag{C.14}$$

$$\phi_n(\beta) \propto \left[\frac{1}{e^{\frac{(\beta-\beta_0)}{a_0}}+1}\right]^{b/2}\left[1-\frac{1}{e^{\frac{(\beta-\beta_0)}{a_0}}+1}\right]^{c/2}P_n^{(b,c)}$$

with

$$b = \frac{1}{2}\left[\sqrt{1+W(4a_0^2)} - (2n+1) + \frac{V(4a_0^2)}{\sqrt{1+W(4a_0^2)} - (2n+1)}\right]$$

$$c = \frac{1}{2}\left[\sqrt{1+W(4a_0^2)} - (2n+1) - \frac{V(4a_0^2)}{\sqrt{1+W(4a_0^2)} - (2n+1)}\right] \tag{C.15}$$

However, in this present consideration,

$$W = \frac{(\frac{L(L+1)}{3} + 2 + \lambda)}{(\beta_0^2)} \left(\frac{48(a_0^2)}{(\beta_0^2)} \right) \tag{C.16}$$

in contrast to the previous case, in which

$$\lambda = \varepsilon_\gamma + \frac{K^2}{3}; \quad \varepsilon_\gamma = (3C)(n_\gamma + 1); \quad n_\gamma = 0,1,2...; \quad C = 2c \; v(\gamma) = (3c)^2 \gamma^2 \tag{C.17}$$

Therefore, the reduced B(E2) rates are [39],

$$R^{B(E2)}_{n,L,n',L'} = \frac{B\left[E2;(L+2)_n \to L'_{n'}\right]}{B\left(E2;2_0 \to 0_0\right)} \tag{C.18}$$

and, consequently

$$B(E2;nLn_\gamma K \to n'L'n_\gamma{}'K') = \frac{5t^2}{16\pi} \left(\left\langle L,2,L' \middle| K,K'-K,K' \right\rangle \right)^2 \Re^2_{n,L,n',L'} \Im^2_{n_\gamma,K,n_\gamma',K'} \tag{C.19}$$

in which

$$\Re_{n,L,n',L'} = \int_0^\infty \beta^5 f_{n',L'}(\beta) f_{n,L}(\beta) d\beta \tag{C.20}$$

and

$$\Im_{n_\gamma,K,n_\gamma',K'} = \int_0^{\pi/3} \cos\gamma \eta_{n'_\gamma,K'}(\gamma) \eta_{n_\gamma,K}(\gamma) \left|\sin 3\gamma\right| d\gamma \quad ; \qquad \Delta K = 0$$

$$\Im_{n_\gamma,K,n_\gamma',K'} = \int_0^{\pi/3} \sin\gamma \eta_{n'_\gamma,K'}(\gamma) \eta_{n_\gamma,K}(\gamma) \left|\sin 3\gamma\right| d\gamma \quad ; \qquad \Delta K = 2 \tag{C.21}$$

PUBLICATIONS

Çapak, M., Gönül, B., (2011), A Search on Two-Electron Atoms, *Journal of Modern Physics*, **2**, 1051-1055

Çapak, M., Cançelik, Y., Ünsal, Ö. L., Atay, Ş., Gönül, B., (2011), An Extended Scenario for the Schrodinger Equation, *Journal of Mathematical Physics*, **52**, 102102

Çapak, M., Gönül, B., (2011), An Alternative Approach to Schrodinger Equations with a Spatially Varying Mass, *Journal of Mathematical Physics*, **52**, 122103

Çapak, M., Petrellis, D., Gönül, B. and Bonatsos, D., (2015), Analytical Solutions for the Bohr Hamiltonian with the Woods-Saxon Potential, *Journal of Physics G: Nuclear and Particle Physics*, **42**, 095102.